Alkaline Benzoquinone Aqueous Flow Battery for Large-Scale Storage of Electrical Energy

Zhengjin Yang, Liuchuan Tong, Daniel P. Tabor, Eugene S. Beh, Marc-Antoni Goulet, Diana De Porcellinis, Alán Aspuru-Guzik, Roy G. Gordon, and Michael J. Aziz**

An aqueous flow battery based on low-cost, nonflammable, noncorrosive, and earth-abundant elements is introduced. During charging, electrons are stored in a concentrated water solution of 2,5-dihydroxy-1,4-benzoquinone, which rapidly receives electrons with inexpensive carbon electrodes without the assistance of any metal electrocatalyst. Electrons are withdrawn from a second water solution of a food additive, potassium ferrocyanide. When these two solutions flow along opposite sides of a cation-conducting membrane, this flow battery delivers a cell potential of 1.21 V, a peak galvanic power density of 300 mW cm^{-2}, and a coulombic efficiency exceeding 99%. Continuous cell cycling at 100 mA cm^{-2} shows a capacity retention rate of 99.76% $cycle^{-1}$ over 150 cycles. Various molecular modifications involving substitution for hydrogens on the aryl ring are implemented to block decomposition by nucleophilic attack of hydroxide ions. These modifications result in increased capacity retention rates of up to 99.96% $cycle^{-1}$ over 400 consecutive cycles, accompanied by changes in voltage, solubility, kinetics, and cell resistance. Quantum chemistry calculations of a large number of organic compounds predict a number of related structures that should have even higher performance and stability. Flow batteries based on alkaline-soluble dihydroxybenzoquinones and derivatives are promising candidates for large-scale, stationary storage of electrical energy.

1. Introduction

The replacement of fossil fuel energy with renewable sources has been increasing as the cost of solar and wind energy falls rapidly. Recent reports show that from 2008 to 2015, the cost of wind generation fell by 41%, rooftop solar photovoltaic installations by 54%, and utility-scale photovoltaic installations by 64%. The cost of solar panels now takes up less than 30% of a fully installed solar electricity system.[1] Although the cost of electricity from wind and sunlight has dropped dramatically, their widespread adoption is impeded by the inherent intermittency of these renewable energy sources. Safe, low-cost, efficient, and scalable energy storage could solve this problem.

A number of energy storage options are available, such as pumped hydro, flywheels, compressed air, supercapacitors, solid-electrode batteries, and redox-flow batteries (RFBs).[2] In RFBs, the redox-active species are separately stored in electrolytes in external tanks, and react reversibly in a device similar to a fuel cell when they are pumped past the electrodes (**Figure 1**A). This design offers significant advantage over solid electrode batteries, by decoupling energy and power output: the former is determined by the tank size and electrolyte concentration, the latter by electrode area.[3] Moreover, aqueous RFBs eliminate the safety issues posed by flammable organic solvents and, due to low electrolyte resistance, enable high current densities. The all-vanadium RFB, which has been the most heavily commercialized, is restricted by the low earth-abundance and the high and fluctuating cost of vanadium.[4] Aqueous organic redox-flow batteries (AORFBs) exploiting water-soluble organic and organometallic redox-active molecules that are composed of only earth-abundant elements[5] have been the subject of recent research. Organic charge-storage materials offer structural diversity, tunable redox potential, and optimizable solubility.[6] High aqueous solubility, well-separated reduction potentials barely avoiding water splitting, stability, safety, and low cost at mass-production scales constitute the most critical attributes for novel aqueous organic electrolytes.

Small molecule-based AORFBs can be run at acidic,[5a] neutral,[3a,5e] or basic pH.[5c,d,7] Substantially higher cell potentials

Dr. Z. Yang, Dr. E. S. Beh,[+] Dr. M.-A. Goulet, Dr. D. De Porcellinis, Prof. R. G. Gordon, Prof. M. J. Aziz
Harvard John A. Paulson School of Engineering and Applied Sciences
29 Oxford Street, Cambridge, MA 02138, USA
E-mail: gordon@chemistry.harvard.edu; maziz@harvard.edu
Dr. Z. Yang
CAS Key Laboratory of Soft Matter Chemistry
iChEM (Collaborative Innovation Center of Chemistry for Energy Materials)
School of Chemistry and Material Science
University of Science and Technology of China
Hefei 230026, P. R. China
L. Tong, Dr. D. P. Tabor, Dr. E. S. Beh, Prof. A. Aspuru-Guzik, Prof. R. G. Gordon
Department of Chemistry and Chemical Biology
Harvard University
12 Oxford Street, Cambridge, MA 02138, USA
The ORCID identification number(s) for the author(s) of this article can be found under https://doi.org/10.1002/aenm.201702056.
[+]Present address: Palo Alto Research Center, 3333 Coyote Hill Road, Palo Alto, CA 94303, USA

DOI: 10.1002/aenm.201702056

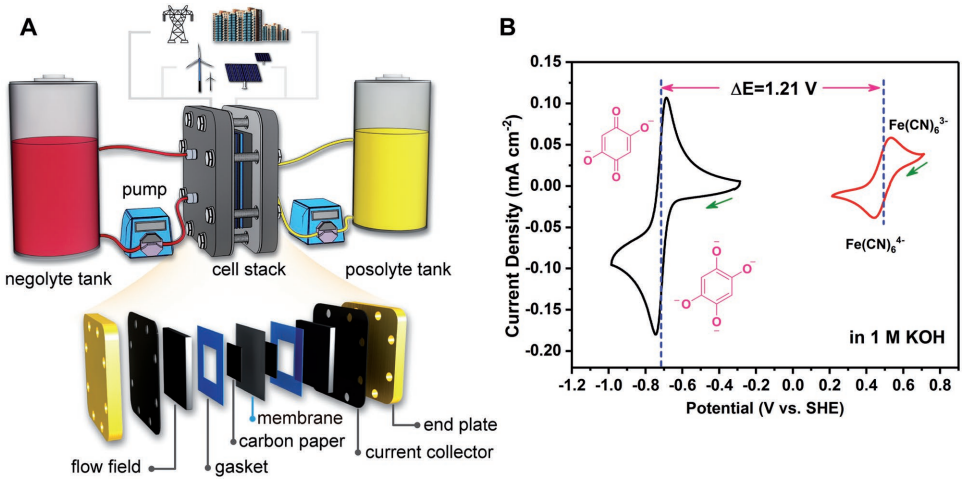

Figure 1. A) Illustration of the AORFB assembled in this contribution. The exploded scheme shows the components of the cell stack. B) Cyclic voltammograms of 1×10^{-3} M potassium ferricyanide/ferrocyanide posolyte ($K_3Fe(CN)_6/K_4Fe(CN)_6$, red line) and 1×10^{-3} M DHBQ/reduced-DHBQ negolyte (black line) in 1 M KOH at a scan rate of 10 mV s^{-1}. Potentials are referenced to the standard hydrogen electrode (SHE). The theoretical cell potential is determined from the difference in reduction potentials (ΔE) of the posolyte and negolyte.

have been demonstrated in basic pH. A current challenge for AORFBs is reaching high energy density (governed by the product of reactant concentration and cell potential) while keeping reactant cost per kWh of energy storage capacity below the corresponding value for vanadium. Anthraquinone-2,7-disulfonate is a negative reactant with high solubility (2.8 M electrons) for an acidic RFB with cost per kWh roughly one-third that of vanadium but, when paired with a bromine/bromide positive reactant, delivers only a modest voltage of 0.81 V[5a] (see also Table S1 and Figure S1, Supporting Information). 2,6-Dihydroxy-anthraquinone has comparable cost and is soluble in alkaline media (1.2 M electrons), where it has been demonstrated as a negative reactant in a 1.20 V cell against $K_4Fe(CN)_6$.[5d] Benzoquinones, which are substantially less expensive than anthraquinones (vide infra), have been utilized in acidic cells: 4,5-dihydroxybenzene-1,3-disulfonic acid[5f,g] and 3,6-dihydroxy-2,4-dimethylbenzenesulfonic acid[5h] have each been paired on the positive electrode with anthraquinone-2,6-disulfonic acid on the negative electrode. To date, these cells have been limited by low voltage, with discharge potential <0.4 V when cycling stably. Here, we report the performance of 2,5-dihydroxy-1,4-benzoquinone (DHBQ) as a promising negolyte (negative electrolyte) material for basic pH. DHBQ is highly soluble in base (>8 M electrons in 1 M KOH) with low reduction potential (–0.72 V vs SHE at pH 14). Although mass production cost is hard to ascertain for new molecules, our investigation of lab-scale reagent grade prices from commercial vendors suggests DHBQ can be obtained at much lower prices than anthraquinones (Table S1 and Figure S1, Supporting Information). We paired DHBQ with potassium ferrocyanide to create an AORFB with a cell potential of 1.21 V. Cells exhibited peak power densities of up to 300 mW cm^{-2}, limited primarily by membrane resistivity, and capacity retention rates upon cycling of up to 99.76% $cycle^{-1}$ over 150 cycles. The capacity loss of 0.24% $cycle^{-1}$ appears to be caused by a combination of DHBQ crossover through the membrane and the chemical instability of DHBQ. Strategies were undertaken to further raise the capacity retention rate. By blocking the unsubstituted carbon atoms in DHBQ, a hydroxylated benzoquinone-based AORFB was attained with improved stability, showing a capacity retention rate of 99.96% $cycle^{-1}$ over 400 consecutive cycles, albeit with increased internal resistance.

2. Results and Discussion

2.1. DHBQ

DHBQ is ubiquitous in cellulose products and is the major survivor of bleaching treatment of cellulose products.[8] It is readily formed from the breakdown of cellulose products and enjoys high resistance toward oxidants such as hydrogen peroxide, ozone, and oxygen by virtue of resonance stabilization[8] (**Figure 2**). The accumulation of negative charge at the unsubstituted positions mitigates possible attack by nucleophilic species (e.g., water or OH^-) through Michael addition, which was proposed to be the major mechanism of capacity fade in an AORFB with a 1,2-benzoquinone-3,5-disulfonic acid posolyte (positive electrolyte).[5g] The combination of chemical resistance and synthetic accessibility of DHBQ made it a logical alternative to investigate.

Initial cyclic voltammetry experiments confirmed that DHBQ undergoes reversible two-electron reduction/oxidation, with well-defined anodic and cathodic peaks having a small peak separation (Figure S2, Supporting Information). In order

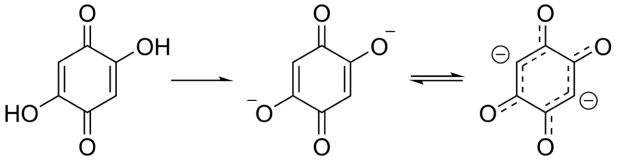

Figure 2. DHBQ and its resonance-stabilized dianions.

for DHBQ to be used in a practical cell, it has to have a high solubility at the operating pH. As expected, DHBQ is highly soluble at high pH due to its two solubility-enhancing hydroxy groups, which are deprotonated above pH 10. UV–vis spectrophotometry of a saturated solution of DHBQ potassium salt in 1 M KOH showed a solubility of 4.31 M (Figure S3, Supporting Information), which corresponds to a negolyte (negative electrolyte) capacity of 231 Ah L^{-1}. A comparison of DHBQ with other reported AORFB negolytes shows that DHBQ enjoys high commercial availability, high solubility, low cost, and low redox potential (Table S1, Supporting Information).

2.2. Effect of pH on DHBQ Redox Behavior

DHBQ behaves differently from other quinones, such as DHAQ.[5d] DHBQ exhibits well-defined anodic and cathodic peaks at pH values of 4 or lower and of 12 or higher (**Figure 3**, Table S2 and Figure S2, Supporting Information), but not in between. At the lowest pH value investigated (0.0, from 1 M H_2SO_4), DHBQ shows well-defined and reversible oxidation and reduction peaks, characterized by a redox potential of 0.41 V versus SHE with an anodic-cathodic peak separation of 40 mV. Increasing the solution pH lowers the redox potential and increases the peak separation, as shown in **Figure 4**, indicating the transition from a reversible reaction to a quasi-reversible reaction. The average slope of the redox potential versus pH over the pH range 0–3.28 is -66 ± 2 mV pH^{-1} unit, which is close to the value of -59 mV pH^{-1} expected from a two-electron, two-proton process. The absolute magnitudes of the peak heights are also consistent with a two-electron process. In the intermediate pH range, we did not observe any electrochemically reversible behavior of DHBQ, with either no oxidation signal or no reduction signal seen upon cycling. Above pH ≈ 11.8, a quasi-reversible redox reaction reemerges, with redox potential of –0.67 V versus SHE and peak separation of 69 mV. When the pH is further increased to 14 (1 M KOH), well-defined reversible oxidation and reduction peaks were again observed, with a redox potential of –0.72 V and a peak separation of 58 mV.

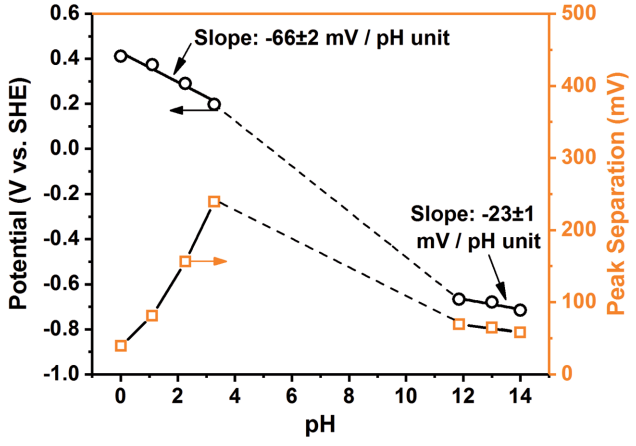

Figure 3. Redox potential and anodic-cathodic peak separation of DHBQ as a function of pH.

2.3. Redox Kinetics of DHBQ

We performed rotating-disk-electrode experiments to evaluate the reduction kinetics of DHBQ, by sweeping negatively from –0.3 to –1.4 V versus SHE. Voltammograms were acquired over a range of rotation rates (Figure 4). A diffusion coefficient (D) of 3.66×10^{-6} cm^2 s^{-1} was determined from a Levich plot of the limiting current versus square root of rotation rate. A Koutecký–Levich plot reveals good linearity of reciprocal electrode currents against the reciprocal square root of rotation rate at different overpotentials from the formal reduction potential ($E^0 = -0.72$ V vs SHE at pH 14). Fitting the kinetically limited current i_k to the Tafel equation yields an electron transfer rate constant (k^o) of 2.12×10^{-3} cm s^{-1}. Compared with other small redox-active molecules, DHBQ shows a diffusion coefficient similar to those of 9,10-anthraquinone-2,7-disulphonic acid,[5a] ferrocene derivatives,[3a] TEMPO derivatives or viologens,[9] and slightly higher than those of the sodium salts of flavin mononucleotide[7] and DHAQ.[5d] As expected, the experimental diffusion coefficient is orders of magnitude higher than that of the redox-active polymers that have been demonstrated in an aqueous RFB.[5b] The electron-transfer rate constant (k^o) is greater than those of ferrocene derivatives,[3a] alloxazine,[5c] methyl viologen,[3b] 4-OH-TEMPO,[3b] V^{3+}/V^{2+}, and VO^{2+}/VO_2^+,[10] comparable to that of flavin mononucleotide,[7] which makes it promising as an AORFB reactant (Table S3, Supporting Information).

2.4. DHBQ/$K_4Fe(CN)_6$ Alkaline AORFB

To demonstrate the capability of DHBQ as the negolyte for an alkaline AORFB, a lab-scale AORFB prototype was assembled using graphite flow plates with serpentine flow fields (see details in the Supporting Information). The positive reservoir (6 mL) comprised of 0.4 M potassium ferrocyanide ($K_4Fe(CN)_6$) in 1 M KOH and the negative reservoir (22.5 mL) was assembled from 0.5 M of DHBQ in 2 M KOH (1 M OH^- was consumed in deprotonating DHBQ). A lower DHBQ concentration than the solubility limit was utilized to ensure osmotic balance with the ferrocyanide posolyte, which has a limited solubility in 1 M KOH. The theoretical cell potential of DHBQ/$K_4Fe(CN)_6$ in 1 M KOH is 1.21 V (Figure 1). We varied the state of charge (SOC) by a constant-coulomb incremental charging technique from 10% to ≈100% and recorded the corresponding open-circuit voltage (OCV) (Figure S4, Supporting Information). The cell potential at 10% SOC is 1.141 V and climbs up to 1.202 V at 50% SOC. The cell voltage reaches 1.255 V at ≈100% SOC.

Initial cell performance was evaluated with three different commercial cation exchange membranes, namely, Nafion 212 (N212), Nafion 115 (N115), and Nafion 117 (N117). Polarization curves (**Figure 5**) show that the cells assembled with N212, N115, and N117 exhibit peak power densities of 300, 164, and 137 mW cm^{-2}, respectively. The difference in peak power density results from the overall cell resistance as reflected in the potential–current curves. The direct current area-specific resistance (DC-ASR) was obtained as the derivative of the potential versus current density curve at OCV. The DC-ASR of the DHBQ/$K_4Fe(CN)_6$ cells with N212, N115, or N117 membranes

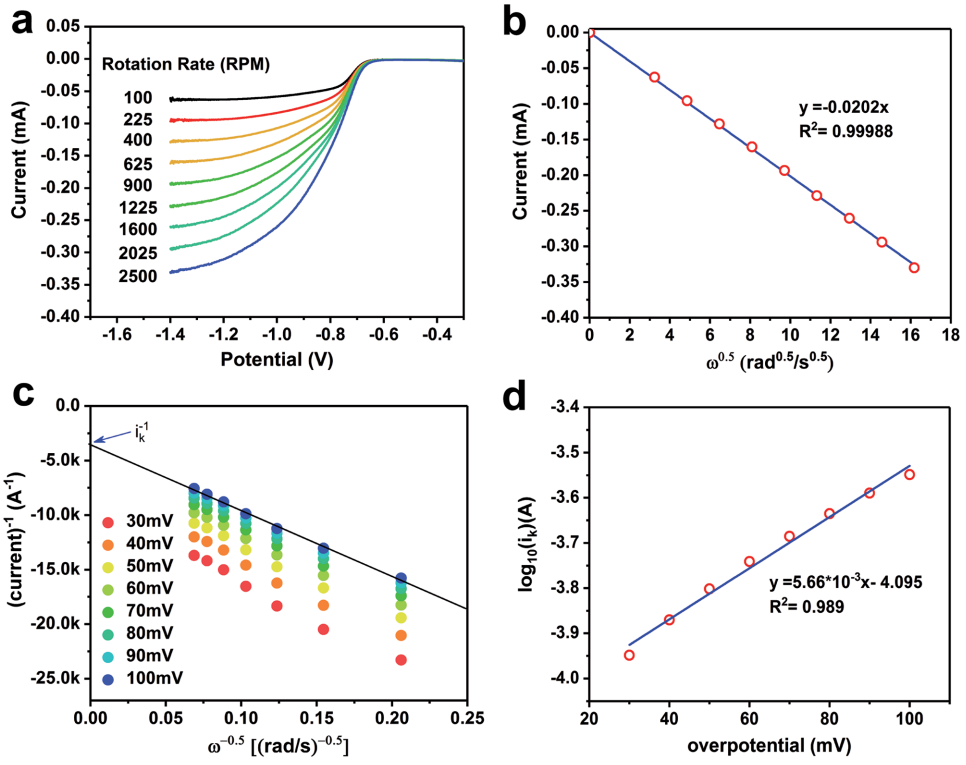

Figure 4. Rotating-disk-electrode (RDE) experiment on DHBQ (1×10^{-3} M in 1 M KOH). a) Current versus potential (referenced to SHE) at rotation rate from 100 to 2500 rpm with potential sweep rate of 5 mV s^{-1}. b) Levich plot of limiting current versus square root of rotation rate ($\omega^{1/2}$). c) Koutecky–Levich plot at different overpotentials; reciprocal of kinetically limited current is indicated on vertical axis. d) Tafel plot, the logarithm of kinetically limited current versus overpotential (potential deviation from the formal reduction potential, referenced to SHE).

was 1.28, 2.41, and 2.85 Ω cm^2, respectively. Electrochemical impedance spectroscopy (EIS) measurements indicate that the membrane resistance is responsible for >85% of the DC-ASR (Figure S5, Supporting Information).

2.5. DHBQ/$K_4Fe(CN)_6$ Cell Cycling

Cell cycling experiments were conducted to evaluate the capacity retention rate of the DHBQ/$K_4Fe(CN)_6$ cell. Prior to cycling, the cell capacity was evaluated with a full charge–discharge process to be 531.4 C, which is 91.8% of the theoretical value (578.9 C in 6 mL negolyte). When cycled galvanostatically at 100 mA cm^{-2} between voltage cutoffs of 1.6 and 0.6 V, the initial capacity was 23.15 Ah L^{-1}, which is 86.4% of the theoretical capacity, 26.79 Ah L^{-1}. We tentatively attribute the value of 91.8% to DHBQ purity and transfer loss, the difference between 91.8 and 86.4% to overpotential during cell cycling. The DHBQ/$K_4Fe(CN)_6$ cell assembled with the N212 membrane suffers from severe capacity fade (Figure S6, Supporting

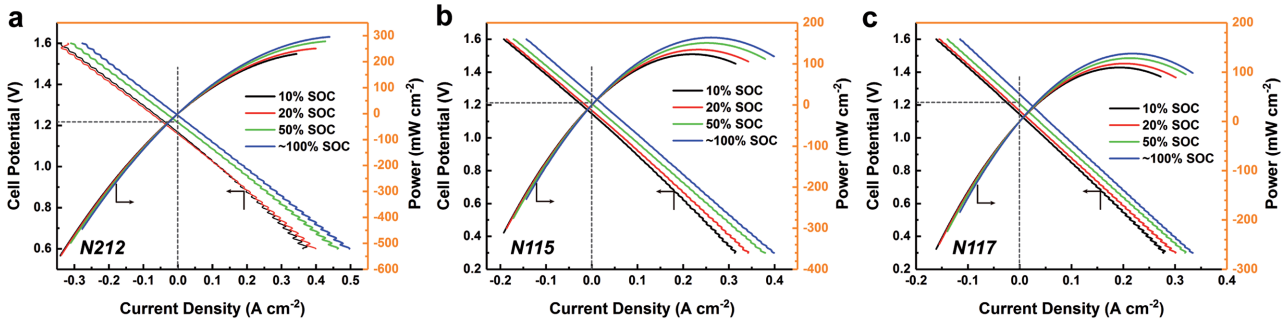

Figure 5. Electrochemical performance of a DHBQ/$K_4Fe(CN)_6$ cell. Electrolytes comprise 6 mL of 0.5 M DHBQ in 2 M KOH (the negolyte) and 22.5 mL of 0.4 M potassium ferrocyanide ($K_4Fe(CN)_6$) in 1 M KOH (the posolyte). The cell-polarization plots, composed of cell potential (left vertical) and power density (right vertical) versus discharge current density, correspond to the cell assembled with a) Nafion 212 membrane (N212), b) Nafion 115 membrane (N115), and c) Nafion 117 membrane (N117). The dashed lines indicate open circuit potential at 50% SOC.

Information). The coulombic efficiency (CE), which is the ratio of the discharge capacity to the immediately preceding charge capacity, is around 77% and drops to 72.5% after 10 cycles. The low value of the CE indicates that self-discharge of the N212 cell is taking place during cycling, which we hypothesize to be caused by crossover of active electrolytes across the membrane. The high DHBQ crossover rate stems from its small molecular size as well as the high water uptake and small thickness of N212 membrane (Table S4, Supporting Information). On the one hand, by switching to thicker membranes, N115 and N117 (**Figure 6**, Figure S7, Supporting Information), a clear increase in the coulombic efficiency of the cell of up to 99% is observed. This coulombic efficiency remains high during cycling, suggesting a reduced membrane crossover rate of the capacity-limiting reagent, DHBQ. The same capacity is obtained at 100 mA cm^{-2} with either the N115 or the N117 membrane, but not with N212. On the other hand, thicker membranes contribute a higher area-specific resistance, as reflected in the polarization curves (Figure 5); high resistance in turn leads to decreased round-trip energy efficiency (EE). The EE of N117-based DHBQ/$K_4Fe(CN)_6$ cell is around 61% at first and stabilizes at ≈56%, whereas it is slightly higher for a N115-based DHBQ/$K_4Fe(CN)_6$ cell and remains comparatively stable at 65%. If the current efficiency loss current is independent of current density, then the EE of the N115 cell can be increased to ≈88% by reducing the current density to 15 mA cm^{-2}—but at an increased capital cost per kW due to the large cell area per unit current.

The capacity retention rates for N115-based and N117-based cells are 99.76 and 99.68% $cycle^{-1}$, respectively. Although the cell remains quite stable from each charge–discharge cycle to the next, the accumulation of the tiny capacity fade during prolonged cycling is not ideal for practical application. The capacity fade rate for the N115-based cell of 0.24% $cycle^{-1}$ extrapolates, assuming exponential decay, to 290 cycles before the capacity drops to 50% of the original, which is inadequate for practical application.

2.6. Capacity Retention Analysis

By reducing the volume of the positive reservoir, a DHBQ/$K_4Fe(CN)_6$ cell that was capacity-limited by the posolyte was assembled and cycled. Results show that discharge capacity of the cell remained unchanged for the first 45 cycles (around 20 h), although the charge capacity varied slightly (Figure S8, Supporting Information). This implies that $K_4Fe(CN)_6$ loss is not contributing to the capacity loss of the DHBQ/$K_4Fe(CN)_6$ cell.

The crossover rate of DHBQ across a N115 membrane was measured in a two-compartment rotating cell (see permeability measurements in the Supporting Information for details). The DHBQ concentration in the receiving reservoir was found to increase linearly over time, indicating a permeability of 1.27×10^{-9} cm^2 s^{-1} (Figure S9, Supporting Information). Considering the time every cycle takes, the effective membrane area and the reservoir volume of the cell, the expected capacity loss caused by DHBQ crossover would be 0.012% $cycle^{-1}$. Although

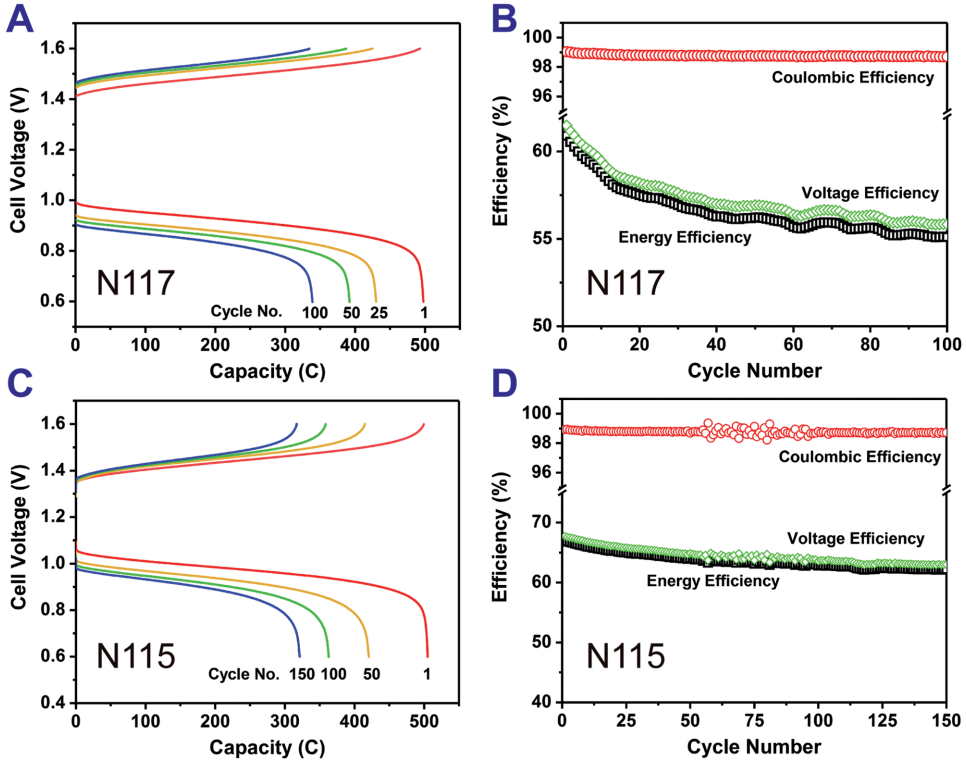

Figure 6. Prolonged galvanostatic cell cycling performance of Nafion-based DHBQ/$K_4Fe(CN)_6$ cell at 100 mA cm^{-2} with potential cutoffs of 1.6 and 0.6 V. No potential holds were employed. The electrolytes comprise 6 mL of 0.5 M DHBQ in 2 M KOH and 22.5 mL of 0.4 M $K_4Fe(CN)_6$ in 1 M KOH. Representative cell potential versus capacity curves (A and B for Nafion 117 membrane, C and D for Nafion 115 membrane) and efficiencies (coulombic efficiency, energy efficiency, and voltage efficiency) over the whole cycling process are presented.

the membrane properties in a static permeability measurement may not permit one to accurately infer its properties in a cycling cell, this is more than an order of magnitude below the observed capacity loss rate in a cycling N115-based DHBQ/$K_4Fe(CN)_6$ cell (0.24% cycle^{-1}). The discrepancy suggests molecular decomposition as a potential mechanism of capacity fade. This hypothesis was then tested by separate experiments, in which the negolyte solution composition after cell cycling, and DHBQ stored in alkaline solutions at elevated temperature, were both analyzed using nuclear magnetic resonance (NMR). A typical ^{1}H-NMR spectrum was too complicated to interpret and suggests the coexistence of multiple species (Figure S10, Supporting Information). However, more information was extracted from the ^{13}C-NMR spectra (Figure S11, Supporting Information). According to the standard spectra of DHBQ in DMSO-d_6 provided by Sigma-Aldrich, two carbon signals should be observed, one at 105 ppm and the other at around 172 ppm; however, the latter is broad and could hardly be observed. After 300 cell cycles, a new peak was observed at 162 ppm, indicating the generation of a new species during cycling. Combined with the information obtained from the ^{1}H-NMR spectrum, we conclude that multiple species are generated during cell cycling although their concentrations are not high enough to be clearly observed in the ^{13}C-NMR spectra. In a separate experiment, in which the oxidized form of DHBQ was subjected to prolonged ex situ alkaline treatment at an extremely elevated temperature of 80 °C for 40 d, no carbon peaks at all could be observed, indicating that DHBQ had degraded chemically. Liquid chromatography-mass spectrometry (LC-MS) analysis of a fresh DHBQ solution shows a single peak at a retention time of 14–15 min, with a mass (m/z) of 139.0037, which agrees exactly with the chemical structure. Although DHBQ could be detected in the LC-MS spectrum of the alkaline-treated DHBQ solution, multiple peaks were observed, which is consistent with the results we obtained in NMR study (Figures S12 and S13, Supporting Information). Despite the fact that LC-MS was able to detect the mass of each peak, we have not yet determined the degradation mechanism. Our working hypothesis is that the chemical decomposition of DHBQ during cell cycling is possibly caused by nucleophilic attack of the hydroxide ions on the unsubstituted carbon atoms of DHBQ.

2.7. Capacity Retention Rate Enhancement

Based on the suspected chemical decomposition mechanism of DHBQ, strategies were then taken to further increase the capacity retention rate of a DHBQ/$K_4Fe(CN)_6$ cell by decreasing the hydroxide concentration in the supporting electrolyte and by blocking the unsubstituted positions in the benzoquinone ring. A DHBQ/$K_4Fe(CN)_6$ cell was run at pH 12 (0.01 M KOH), at which DHBQ still exhibits well-defined reversible oxidation and reduction peaks (Figure S2, Supporting Information) despite its reduced solubility (around 0.3 M electrons, Figure S3, Supporting Information) compared to at pH 14. The cell potential remains close to that of the cell run at pH 14. Galvanostatic charge–discharge cycling was conducted at 40 mA cm^{-2} and the evolution of the overall cell capacity was evaluated by fully charging and then fully discharging the cell once every ten cycles (Figure S14, Supporting Information). The overall discharge capacity retention rate was 99.98% cycle^{-1}, which extrapolates, assuming exponential decay, to over 3400 cycles before the capacity decays to 50% of its initial value. The results confirm the effectiveness of enhancing capacity retention of DHBQ/$K_4Fe(CN)_6$ cell at lower OH^- concentration.

It has been proposed that the degradation of benzoquinones in acidic conditions is caused by Michael addition,[5g] which can be mitigated by a blocking strategy.[5h] In basic pH, hydroxide ions are stronger nucleophiles than water is in acid. Synthetic efforts were made to verify the effectiveness of improving the chemical stability of DHBQ by blocking the unsubstituted positions. 3,6-Bis(diphenylmethyl)-2,5-dihydroxy-1,4-benzoquinone (DPM-DHBQ) was synthesized using a reported procedure and characterized by cyclic voltammetry (see the Supporting Information for details). Results indicate that DPM-DHBQ is redox-active and the reduction and re-oxidation occur at −1.0 and −0.5 V, respectively, showing a half-wave potential of roughly −0.75 V versus SHE (Figure S15, Supporting Information). The redox potential is close to that of DHBQ, and the peaks remain unchanged during repeated scans. However, adding extra aromatic rings to block the unsubstituted carbon atoms led to an increased peak separation in the CV, implying sluggish redox kinetics on glassy carbon. Incorporating extra aromatic rings also caused a severe decrease in solubility that precluded full cell studies. Considering the acquired facts and synthetic difficulties, molecular simulations were conducted to help understand the behavior of blocked DHBQ molecules and are presented in a later section.

Alternatively, the vulnerable 3- and 6-positions on DHBQ can also be blocked by polymerization. The polymerization of benzoquinone in alkaline solutions (polyBQ, see the Supporting Information for details) and the acid-catalyzed condensation of DHBQ with formaldehyde[11] generate polymers that have repeating units with a similar structure to DHBQ. Furthermore, we anticipate such structures would be redox-active but no longer susceptible to nucleophilic attack.

A polyBQ/$K_3Fe(CN)_6$ cell was assembled and run at pH 14 (potassium ferricyanide, $K_3Fe(CN)_6$ was utilized because polyBQ is produced in its reduced form). Similarly, the constant-coulomb incremental charging technique was utilized and the open-circuit voltage at 10% SOC is 0.806 V, which increases to 1.279 V at ≈100% SOC (Figure S16, Supporting Information). The potential at 50% SOC, 1.004 V, is lower than that of the DHBQ/$K_4Fe(CN)_6$ cell. Polarization curves show that the peak power density of the polyBQ/$K_3Fe(CN)_6$ cell at ≈100% SOC is ≈30 mW cm^{-2} (Figure S17, Supporting Information). The low peak power density is because of the extremely high overall resistance (DC-ASR), which is over 9 Ω cm^2; the resistance is four times that of the DHBQ/$K_4Fe(CN)_6$ cell with the same membrane. In situ EIS measurements showed that the high-frequency resistance of the cell (Figure S18, Supporting Information) was more than doubled by the replacement of DHBQ with polyBQ. Based on our established resistance model,[12] the high-frequency resistance is dominated by the membrane resistance, which may have suffered increases due to the plugging of ionic transport channels by polyBQ. It is also possible that polymerization has reduced the ionic diffusivity in the electrolyte to the point that mass transfer limitations have become important.

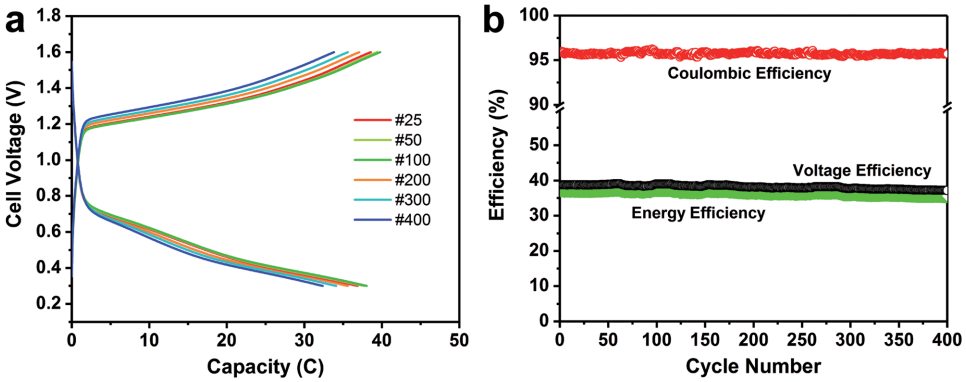

Figure 7. Cell cycling performance of a polyBQ/$K_3Fe(CN)_6$ cell utilizing Nafion 115. Due to a higher overall resistance, the cell was cycled at 10 mA cm^{-2} with potential cutoffs of 1.6 and 0.6 V, without any potential holds. Representative cell potential versus a) capacity curves and b) efficiencies over 400 consecutive cycles are presented.

The assembled polyBQ/$K_3Fe(CN)_6$ cell was cycled for 400 cycles at 10 mA cm^{-2} (**Figure 7**). The CE and EE at 10 mA cm^{-2} were 96% and 37%, respectively and remained unchanged over 400 cycles, indicating a stable charge–discharge process. The capacity of the cell is ≈25% of the theoretical capacity, which may be due to the coil conformation and chain entanglement of polyBQ in solution, as well as the slower kinetics compared with small molecules. In the meantime, the increase in viscosity due to increased molecular size also reduces the contact of redox-active repeating units to the electrodes. During the first 100 cycles, the capacity is slightly variable and increases slightly. During the following 300 cycles, the capacity retention rate was 99.962% $cycle^{-1}$ (Figure 7a). Compared with the highest capacity retention rate we acquired for a N115-based DHBQ/$K_4Fe(CN)_6$ cell (99.76% $cycle^{-1}$), the improvement in capacity retention rate supports our hypothesis about the effectiveness of the blocking strategy. We believe further increase in capacity retention rate can be achieved by incorporating poly(2,5-dihydroxyl-1,4-benzoquinone-3,6-methylene), the polymer from acid-catalyzed condensation of DHBQ with formaldehyde (Figure S19, Supporting Information), as negolyte. Although the reaction was claimed to be readily carried out,[11] we have encountered more difficulties than expected in acquiring the polymeric products. Future research effort will focus on understanding the difference in redox behavior between the monomer and its polymer counterpart. Synthetic efforts will also be devoted to acquiring the most promising substituted DHBQ based on theoretical modeling and evaluating the electrochemical properties.

2.8. Theoretical Modeling and Screening

Given the promise of DHBQ, we conducted a virtual screening of modified DHBQ molecules to identify potential improvements, understand potential effects of polymerization at the monomer level, and gain insights about the chemical space in the vicinity of the molecule. For this work, two properties were considered, the first being the reduction potential versus DHBQ and the second being the redox behavior. Molecules that exhibit a one-step $2e^-$ oxidation/reduction behavior in computed processes are favored, because reactive radical intermediates might be generated during a two-step sequence of $1e^-$ oxidation/reduction processes. Thus, we seek to minimize the overall two-electron reduction potential (without promoting conditions that evolve H_2), while also maintaining the one-step $2e^-$ oxidation/reduction in simulation and maximize solubility. A full list of the results for the screened molecules can be found in Tables S5 and S6, Figures S20–S22 (Supporting Information); in **Table 1** we report the most promising molecules. The molecules in Table 1 satisfy the following criteria: a cell voltage more than 0.1 V higher than that of DHBQ when paired with ferrocyanide (i.e., a reduction potential more than 0.1 V lower than DHAQ), a predicted solubility of >1 M (Log$S$ > 0), and predicted to be a one-step reduction.

Here, we discuss some illustrative cases. First, DHBQ derivatives with alkyl substitutions were explored to elucidate

Table 1. Calculated reduction potentials for most promising DHBQ derivatives.

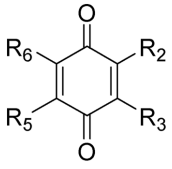

R_2, R_5	R_3, R_6	Predicted $2e^-$ reduction potential[a] [V]	Predicted oxidized form Log$S$ at pH = 14[b]
−OH	$-CH_2N(CH_3)_2$	−0.25	1.91
−OH	$-(CH_2CH_2O)_4-H$	−0.21	2.65
−OH	$-CH_2NH_2$	−0.18	2.28
−OH	$-(CH_2CH_2O)_3-H$	−0.15	2.56
−OH	$-CH_2CH_3$	−0.15	0.14
$-(O-CH_2CH_2)_2-OH$	$-CH_2NH_2$	−0.14	0.08
−OH	$-CH_2CH_2NH_2$	−0.14	2.45
−OH	$-CH_3$	−0.12	1.49
$-(O-CH_2CH_2)_2-OH$	$-CH_2CH_2NH_2$	−0.12	0.30

[a]Calculated versus DHBQ using B3LYP/6-311+G(d,p) CPCM; [b]Calculated using ChemAxon suite.

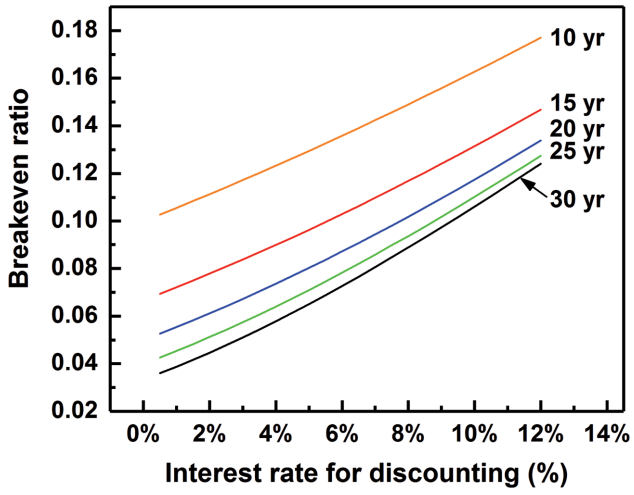

Figure 8. Breakeven ratio of annual replacement cost to savings in capital cost versus interest rate for discounting. A 10–30 year project life is assumed.

the differences in the reduction potential between the subunits of polymers and the DHBQ monomer. In general, in the addition of shorter alkyl chains reduces the reduction potential relative to DHBQ, though there are some instances in Table S6 (Supporting Information) where alkyl substitutions on DHBQ would lower the cell potential. From the group with shorter alkyl chain substitutions, the molecule in Table 1 with two $CH_2N(CH_3)_2$ substitutions is predicted to have the highest cell voltage (see Tables S5 and S6, Supporting Information, for a list of some of the compounds considered).

Second, we considered modifications of the OH groups on DHBQ (in conjunction with the other substitutions), including substituting them with polyether chains. Interestingly, the substitution of a single polyethylene glycol subunit typically decreases the cell voltage relative to DHBQ, whereas the replacement of OH by a two or three-unit polyethylene glycol chain increases the cell voltage. We also examined the substitution of the non-OH sites with similar chains and found that when combining two OH groups with a pair of three ethylene glycol chain substitutions, the cell voltage is predicted to be 0.21 V higher than that of DHBQ. Based on this and the predicted solubility in basic solution, this molecule appears to be one of the most promising in this group.

The ultimate goal for organic flow battery reactants is to achieve sufficient stability at a reasonable cost. For long-lifetime projects such as flow batteries for grid storage, discounting can become an important consideration. If the present value of the accumulated annual replacement cost is less than the savings in capital cost compared to vanadium then, other things being equal, the low-cost, shorter-lived reactant is the lower-cost option. This is illustrated in **Figure 8**, which displays the breakeven point for the ratio of the annual replacement cost to the capital cost savings between a lower cost organic electrolyte and a higher cost infinitely stable reactant. For example, if the infinite-life electrolyte cost is 50$ kWh^{-1} and the low-cost organic reactant costs 10$ kWh^{-1} but requires 30% be replaced per year, the breakeven ratio is (30% × 10)/(50–10) = 7.5%. For a 20-year project, replacement of the cheaper shorter-lived reactant becomes the economically favorable choice when the interest rate for discounting exceeds 4%. This requires, of course, that decomposition products do not compromise the battery performance and that replacement is technically achievable and has negligible additional associated costs. We propose that benzoquinone functionalization, similar to the one presented in this study, is a promising path toward achieving this commercialization goal.

3. Conclusions

Our results indicate that DHBQ-based reactants are promising for alkaline organic RFBs. Compared with anthraquinone-based reactants, benzoquinones have higher alkaline solubility, lower molecular weight, and lower cost. The lower molecular weight, however, causes enhanced membrane permeability and thereby poses challenges for membrane development toward low molecular permeability while maintaining high ionic conductivity, in order to prevent capacity fade due to molecular crossover. Fortunately, many membranes now available seem to be sufficiently stable up to pH 14. DHBQ, without further substitution, is not sufficiently stable to provide the service life needed for practical implementation. Our observations support the hypothesis that nucleophilic attack of hydroxide ions on the unsubstituted carbon atoms of the DHBQ aryl ring is responsible for the observed capacity fade. Synthesized derivatives of DHBQ, in which the aryl ring is fully substituted in various ways, substantially altered the capacity retention rate as well as the solubility and redox activity. The insight gained from computational screening, in conjunction with these experiments, points out avenues for further performance improvement and give us a fighting chance of using benzoquinone-based alkaline organic RFBs to provide safe, cost-effective, robust stationary electrical energy storage.

Supporting Information

Supporting Information is available from the Wiley Online Library or from the author.

Acknowledgements

Z.Y. and L.T. contributed equally to this work. Z.Y. greatly appreciates financial support from the National Science Foundation of China (No. 21506201) and a scholarship from the China Scholarship Council to study at Harvard University. This work was supported in part by the following organizations: the U.S. Department of Energy Contract No. DE-AC05-76RL01830 through PNNL Subcontract No. 304500; ARPA-E Award No. DE-AR0000348; National Science Foundation grant No. CBET1509041; the Harvard School of Engineering and Applied Sciences and the Massachusetts Clean Energy Technology Center. The authors thank Dr. Michael R. Gerhardt, Dr. David Kwabi, and Andrew Wong for assistance and helpful discussions on experimental electrochemical techniques.

Conflict of Interest

The authors declare no conflict of interest.

Keywords

alkaline aqueous flow batteries, benzoquinone, energy storage, molecular simulation

Received: July 27, 2017
Revised: September 11, 2017
Published online:

[1] a) B. Obama, *Science* **2017**, *355*, 126; b) N. S. Lewis, *Science* **2016**, *351*, aad1920.
[2] a) J. Winsberg, T. Hagemann, T. Janoschka, M. D. Hager, U. S. Schubert, *Angew. Chem., Int. Ed. Engl.* **2017**, *56*, 686; b) P. Alotto, M. Guarnieri, F. Moro, *Renewable Sustainable Energy Rev.* **2014**, *29*, 325.
[3] a) B. Hu, C. DeBruler, Z. Rhodes, T. L. Liu, *J. Am. Chem. Soc.* **2017**, *139*, 1207; b) T. Liu, X. Wei, Z. Nie, V. Sprenkle, W. Wang, *Adv. Energy Mater.* **2016**, *6*, 1501449; c) M. Park, J. Ryu, W. Wang, J. Cho, *Nat. Rev. Mater.* **2016**, *2*, 16080.
[4] a) C. J. Barnhart, S. M. Benson, *Energy Environ. Sci.* **2013**, *6*, 1083; b) M. Armand, J. M. Tarascon, *Nature* **2008**, *451*, 652.
[5] a) B. Huskinson, M. P. Marshak, C. Suh, S. Er, M. R. Gerhardt, C. J. Galvin, X. Chen, A. Aspuru-Guzik, R. G. Gordon, M. J. Aziz, *Nature* **2014**, *505*, 195; b) T. Janoschka, N. Martin, U. Martin, C. Friebe, S. Morgenstern, H. Hiller, M. D. Hager, U. S. Schubert, *Nature* **2015**, *527*, 78; c) K. Lin, R. Gómez-Bombarelli, E. S. Beh, L. Tong, Q. Chen, A. Valle, A. Aspuru-Guzik, M. J. Aziz, R. G. Gordon, *Nat. Energy* **2016**, *1*, 16102; d) K. Lin, Q. Chen, M. R. Gerhardt, L. Tong, S. B. Kim, L. Eisenach, A. W. Valle, D. Hardee, R. G. Gordon, M. J. Aziz, M. P. Marshak, *Science* **2015**, *349*, 1529; e) E. S. Beh, D. De Porcellinis, R. L. Gracia, K. T. Xia, R. G. Gordon, M. J. Aziz, *ACS Energy Lett.* **2017**, *2*, 639; f) B. Yang, L. Hoober-Burkhardt, F. Wang, G. S. Prakash, S. Narayanan, *J. Electrochem. Soc.* **2014**, *161*, A1371; g) B. Yang, L. Hoober-Burkhardt, S. Krishnamoorthy, A. Murali, G. S. Prakash, S. Narayanan, *J. Electrochem. Soc.* **2016**, *163*, A1442; h) L. Hoober-Burkhardt, S. Krishnamoorthy, B. Yang, A. Murali, A. Nirmalchandar, G. K. S. Prakash, S. R. Narayanan, *J. Electrochem. Soc.* **2017**, *164*, A600.
[6] S. Er, C. Suh, M. P. Marshak, A. Aspuru-Guzik, *Chem. Sci.* **2015**, *6*, 885.
[7] A. Orita, M. G. Verde, M. Sakai, Y. S. Meng, *Nat. Commun.* **2016**, *7*, 13230.
[8] T. Hosoya, A. French, T. Rosenau, *Mini-Rev. Org. Chem.* **2013**, *10*, 309.
[9] T. Janoschka, N. Martin, M. D. Hager, U. S. Schubert, *Angew. Chem., Int. Ed. Engl.* **2016**, *55*, 14427.
[10] T. Yamamura, N. Watanabe, T. Yano, Y. Shiokawa, *J. Electrochem. Soc.* **2005**, *152*, A830.
[11] T. Le Gall, K. H. Reiman, M. C. Grossel, J. R. Owen, *J. Power Sources* **2003**, *119*, 316.
[12] Q. Chen, L. Eisenach, M. J. Aziz, *J. Electrochem. Soc.* **2015**, *163*, A505 7.

ADVANCED ENERGY MATERIALS

Supporting Information

for *Adv. Energy Mater.,* DOI: 10.1002/aenm.201702056

Alkaline Benzoquinone Aqueous Flow Battery for Large-Scale Storage of Electrical Energy

Zhengjin Yang, Liuchuan Tong, Daniel P. Tabor, Eugene S. Beh, Marc-Antoni Goulet, DianaDe Porcellinis, Alán Aspuru-Guzik, Roy G. Gordon, and Michael J. Aziz**

Supplementary information for

Alkaline benzoquinone aqueous flow battery for large-scale storage of electrical energy

Zhengjin Yang[a,c]†, Liuchuan Tong[b]†, Daniel P. Tabor[b], Eugene S. Beh[a,b,d], Marc-Antoni Goulet[a], Diana De Porcellinis[a], Alán Aspuru-Guzik[b], Roy G. Gordon[a,b]*, Michael J. Aziz[a]*

[a] Harvard John A. Paulson School of Engineering and Applied Sciences, 29 Oxford Street, Cambridge, Massachusetts 02138, USA
[b] Department of Chemistry and Chemical Biology, Harvard University, 12 Oxford Street, Cambridge, Massachusetts 02138, USA
[c] CAS Key Laboratory of Soft Matter Chemistry, *i*ChEM (Collaborative Innovation Center of Chemistry for Energy Materials), School of Chemistry and Material Science, University of Science and Technology of China, Hefei 230026, P.R. China
[d] Current address: Palo Alto Research Center, 3333 Coyote Hill Road, Palo Alto, CA 94303

*Corresponding authors:

Roy G. Gordon
Cabot Professor
Dept. of Chemistry and Chemical Biology
12 Oxford Street, MA 02138, USA
Tel: +1 617-495-4017
Fax: +1 617-495-4723
email: Gordon@chemistry.Harvard.edu

Michael J. Aziz
Gene and Tracy Sykes Professor of Materials and Energy Technologies
Harvard John A. Paulson School of Engineering and Applied Sciences, Pierce Hall 204a
29 Oxford Street, MA 02138, USA
Tel: +1 (617) 495-9884
email: maziz@harvard.edu

† These authors contributed equally.

General information for synthesis. ^{1}H NMR and ^{13}C NMR spectra were recorded on Varian INOVA 500 spectrometers. NMR spectra were recorded in solutions of deuterated chloroform ($CDCl_3$) with the residual chloroform (7.24 ppm for ^{1}H NMR and 77.1 ppm for ^{13}C NMR) taken as the internal standard, deuterated dimethyl sulfoxide (DMSO-d_6) with the residual dimethyl sulfoxide (2.49 ppm for ^{1}H NMR and 39.5 ppm for ^{13}C NMR) taken as the internal standard, and were reported in parts per million (ppm).

All solvents and reagents were purchased from Sigma-Aldrich, Alfa Aesar, or Oakwood Chemical, and were used as received unless otherwise specified.

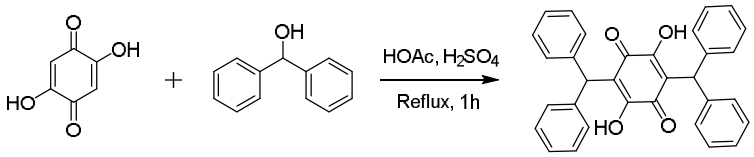

Scheme 1. Synthesis of **DPM-DHBQ**.

3,6-Bis(diphenylmethyl)-2,5-dihydroxy-1,4-benzoquinone (DPM-DHBQ). The synthesis of **DPM-DHBQ** was carried out according to reported procedure (**Scheme 1**)[1]. 2,5-dihydroxybenzoquinone (DHBQ, 2.00 g, 14.3 mmol), diphenylmethanol (5.50 g, 29.9 mmol) and concentrated sulfuric acid (0.5 mL) were refluxed for 1 h in 20 mL of acetic acid. The resulting solution was cooled to room temperature and the product precipitated out. The precipitate was crushed with a spatula and collected by vacuum filtration. The collected yellow crystals were washed with a small amount of acetic acid and then with DI water. The product was finally dried overnight in air at 95 °C. To ensure purity for electrochemical study, it was further purified by recrystallization from acetic acid. NMR of the product matched previously reported values in the literature. ^{1}H-NMR ($CDCl_3$, 500MHz, ppm): 5.7 (s; 2 H), 7.2-7.3 (m; 20 H), 7.9 (s; 2 H).

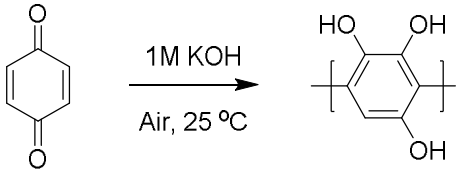

Scheme 2. Polymerization of benzoquinone in aqueous alkali (1 M KOH, bubbled air, room temperature)

Polybenzoquinone (PolyBQ). PolyBQ was synthesized according to published procedure (**Scheme 2**)[2]. Benzoquinone (2.70 g, 25 mmol) was added to aqueous KOH (25 mL, 1 M) and a considerable amount of heat was immediately generated. The mixture was vigorously stirred and cooled to room temperature. The reaction vessel was sealed with a septum and air was driven through the solution via a needle.

To prevent the loss of water, the gas inlet was connected to a bubbler containing a solution of 1 M KOH. After 24 h of reaction, concentrated HCl was added and the neutralized solution was cooled. The precipitated polymer was collected by filtration, washed with DI water and finally dried at 90 ^{o}C under vacuum for 6 h.

Methods

Cyclic voltammetry (CV) was conducted on a Gamry Reference 3000 potentiostat (Gamry Instruments, United States) using three-electrode technique, with glassy carbon as the working electrode, Pt wire as the counter electrode and a Ag/AgCl (BASi®, MF-2052, 3 M NaCl filling solution) reference electrode. All the electrodes were obtained from BASi® (United States). The potential of the Ag/AgCl reference electrode is +0.213 V versus the standard hydrogen electrode (SHE). Cyclic voltammograms (CVs) of 1mM DHBQ were obtained in solutions containing 1 M NaCl as supporting electrolyte, adjusted to the desired pH by adding 1 M KOH or 1 M H_2SO_4. CVs performed in 1 M KOH and 1 M H_2SO_4 were considered to have been performed at pH 14 and pH 0, respectively.

Rotating-disk-electrode (RDE) measurements. RDE experiments on 1 mM DHBQ in 1 M KOH were carried out using a Gamry Reference 3000 potentiostat and a Pine E4TQ RDE. A 5-mm diameter glassy carbon rotating electrode was utilized and the solution was thoroughly purged with argon (30 mins). For RDE experiments, the potential of the rotating-electrode was swept from -0.5 V to -1.65 V (referenced to Ag/AgCl, BASi®, MF-2052) at a sweep rate of 5 mV/s with rotational speeds between 100-2500 rpm. At each rotation speed, three separate linear sweep voltammetry experiments were performed and averaged to acquire the kinetics parameters. Background scans were also taken with blank supporting electrolyte solution (1 M KOH) and subtracted. The limiting currents were measured at -1.4V vs SHE. The Levich equation, Koutecký–Levich equation and Tafel equation[3] were used to deduce the standard kinetic rate constant (k^0, cm/s), the transfer coefficient (α) and

diffusion coefficient (D, cm^2/s). Other involved parameters include: number of electrons transferred, $n = 2$; Faraday's constant, $F = 96485$ C/mol; electrode area, $A = 0.1963$ cm^2; DHBQ concentration, $c = 1\times10^{-6}$ mol/cm^3; kinematic viscosity, $\upsilon = 0.01$ cm^2/s.

LC-MS. High-resolution LC-MS analyses of DHBQ decomposition was performed in the Small Molecule Mass Spectrometry Facility on a Bruker Impact II q-TOF with internal calibration sodium formate clusters. Liquid chromatography was performed on an Agilent 1290 Infinity HPLC using a Dikma Platisil PH column (150mm, 5um particle size, 4.6mm ID, catalog number 99510) at a flow rate of 0.4 mL/min and the following elution conditions were applied: 100% solvent A for 2 min, a gradient increasing from 0% to 15% solvent B in solvent A over 13 min, a gradient increasing to 100% solvent B over 5 min, a gradient decreasing to 0% solvent B in solvent A over 0.1 min, and 100% solvent A for 4.9 min (solvent A = 0.1% v/v formic acid in water; solvent B = 0.1% v/v formic acid in acetonitrile). The ESI mass spectra were recorded in negative ionization mode.

Full-cell testing. Cell hardware was purchased from Fuel Cell Tech (Albuquerque, NM) and pyrosealed POCO graphite flow plates with serpentine flow fields were used for both sides. The electrodes each comprised 4 stacked sheets of Sigracet SGL 39AA carbon paper electrodes (baked at 400 $^{\circ}$C for 24 h before use) of 5 cm^2 geometric area. A Nafion membrane (DuPont, N212, N117, or N115) sandwiched between the positive and the negative electrodes. The space between the flow plates was well-sealed with Viton gaskets. The electrolytes were pumped through PFA tubing (1/8" ID) into and out from the cell stack using Cole-Parmer Micropump peristaltic pumps at a rate of 60 rpm. The cell was placed in a glove bag and high purity nitrogen was used to repeatedly flush oxygen out of the system prior to any experiments. A steady nitrogen flow was maintained during cell cycling. Galvanostatic cell cycling was performed at 500 mA (100 mA/cm^2), with voltage cutoffs of 0.6 and 1.6 V,

controlled by a Bio-Logic BCS-815 cell testing apparatus. Polarization curves were acquired by charging the cell to certain states of charge (SOC), then polarized by linear sweep voltammetry at 100mV/s. This technique has been found to yield polarization curves similar to point-by-point galvanostatic holds, but yet has minimal influence on the cell SOC. Potentio-controlled electrochemical impedance spectroscopy (PEIS) was recorded as needed at frequencies ranging from 1 Hz – 10 kHz.

Solubility tests. The solubility limit of DHBQ in 0.01 M KOH and 1 M KOH were measured by adding the potassium salt of DHBQ (prepared by reacting DHBQ with potassium ethoxide in ethanol, followed by filtration) until no further solid could be dissolved. After filtering the mixture through a PTFE 0.45μm syringe filter, a saturated solution of DHBQ in KOH was obtained. The saturated solution was then diluted by a known amount and the concentration was evaluated by UV-Vis (Agilent Cary 60 spectrophotometer) at 320 nm. The concentration was calculated according to a pre-calibrated absorbance-concentration curve of known concentrations of DHBQ.

Permeability measurements. The permeability of DHBQ across the membrane was evaluated with a lab-made two compartment cell[4]. The donating side was filled with a solution of DHBQ (0.5 M) in KOH (1 M) and the receiving side was filled with 1 M KOH. Both compartments had the same volume. The cell was continuously agitated on a nutating table. At different time intervals, aliquots were taken from the receiving side, diluted and characterized by UV-Vis spectrophotometry. The concentration was calculated from a calibration curve. The permeability was then calculated based on Fick's law, using equations as follows.

$$P = \frac{c_t V_0 l}{At(c_0 - c_t)} \approx \frac{c_t V_0 l}{Atc_0}$$

Where, P is the permeability (cm^2/s), A is the effective area of the membrane (0.942 cm^2), t is the elapsed time (s), c_t is the concentration of active species in the receiving side at time t (mol/L), V_0 is the volume of the solution in either compartment (5 cm^3), l is the thickness of the membrane (127 μm), and c_0 is the concentration of DHBQ in the donating side (0.5 mol/L).

Computational methods. For each candidate molecule in the virtual screening library, up to 20 conformers were generated for the molecules using the MMF94 force field. From these conformers, optimized geometries were found for the oxidized, singly-reduced radical, and doubly-reduced closed-shell molecule at the B3LYP/6-31+G(d) level of theory. At these optimized geometries, the energy was evaluated with a single point calculation at the B3LYP/6-311+G(d,p) level of theory in a polarizable continuum model (PCM) implicit solvent using Bondi atomic radii. All electronic structure calculations used the QChem 4.2 electronic structure package[5]. Since this level of theory has systematic errors in calculating the redox potentials of anions, the first and second reduction potentials were calibrated against the first and second reduction potentials for a set of 116 substituted benzoquinones calculated by Hunyh et al. [6]. Their calculations include an optimization with the PCM solvation model, zero-point effects, and thermodynamic corrections to free energies. We find that for all benzoquinones that do not contain carboxylic acid or thiol substitutions, the protocol outlined above is of sufficient quality on both the first and second reduction potentials to be used in the screening (Supplementary Fig.S20 and Fig.S21). Since larger negative charges (beyond a net charge of -2) would be prone to even larger systematic errors in the electron affinities, our calculations were performed with all substituents on the DHBQ derivatives neutralized, despite the likely presence of their deprotonated forms in base. Thus, all reduction potentials are relative to the form of DHBQ where the non-redox-active OH groups are protonated, which maximizes error cancellation. The solubility of the oxidized form of each molecule was estimated using the Calculator Plugins tool of the ChemAxon suite [7].

Table S1. Overview of reported negolytes for aqueous organic flow battery and lab-scale reagent grade prices [a].

Negative electrolyte	FW (g/mol)	Potential (V vs.SHE)	Solubility (mol/L)	No. of electrons delivered	Year of Publication	Cost/Sources ($/g)
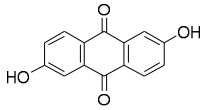 2,6-dihydroxyanthraquinone (DHAQ)	240.2	-0.68 (pH 14)	0.6 M	2	2015[8]	Sigma:19.3 TCI: 59.4 AK: 11.2
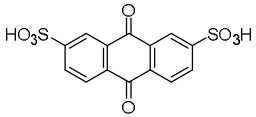 9,10-anthraquinone-2,7-disulphonic acid AQDS	368.3	0.22 (pH 0)	1.5 M	2	2014[9]	Sigma: 6.6 TCI: 28.2 AK: 12.9
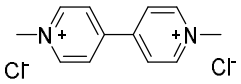 Methyl viologen (MV)	257.2	-0.45 (pH 7)	3.0 M	1	2016[10]	Sigma:46.8

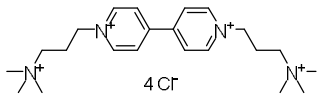 (3-trimethylammonio)propyl viologen tetrachloride (BTMAP-Vi)	500.4	-0.34 (pH 7)	2.0 M	1	2017[4]	3-step lab synthesis
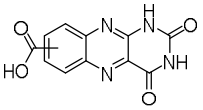 Alloxazine 7/8-carboxylic acid (ACA)	258.2	-0.62 (pH 14)	0.5 M	2	2016[11]	1-step lab synthesis
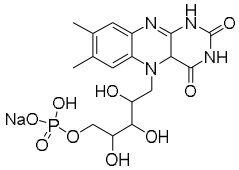 Riboflavin-5'-monophosphate sodium salt (FMN-Na)	480.4	-0.52 (pH 14)	0.24 M	2	2016[3b]	Sigma: 3.5 TCI: 3.2 AK: 2.8
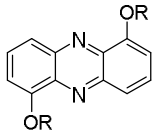 (R is PEGylated TEMPO) Phenazine	785.0	-0.39 (pH 7)	10 mM	2	2016[12]	4-step lab synthesis

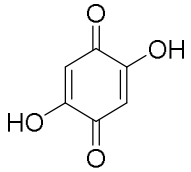 DHBQ	140.1	-0.72	4.31 M	2	This work	Sigma: 2.06 TCI: 2.68 AK: 5.44

[a] Although mass production cost is hard to ascertain for new molecules, the predicted cost vs. quantity curve (Fig. S1, from a consulting company) suggests that the price could be much lower if mass production is guaranteed.

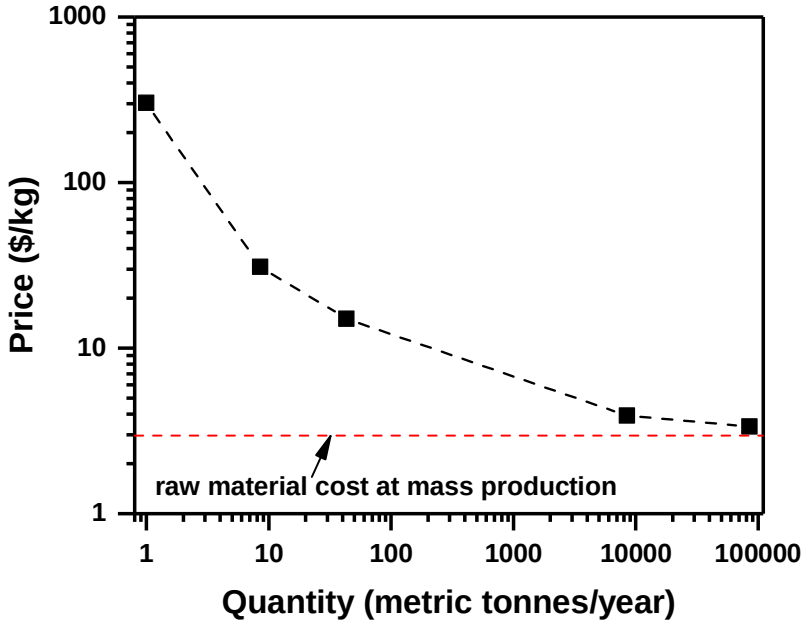

Figure S1. Prediction of anthraquinone (2,6-DHAQ and AQDS) mass production cost as a function of quantity (Sources: Borealis Technology Solutions LLC)

Table S2. Redox potential and anodic-cathodic peak separation of DHBQ as a function of pH.

pH[a]	Redox Potential [b] ($E_{1/2}$, V vs. SHE)	CV Peak Separation (ΔE, mV)
0	0.41	40
1.10	0.37	81
2.27	0.29	156
3.28	0.20	240
11.85	-0.67	69
13	-0.68	65
14	-0.72	58

[a] The investigated pH ranges 0 to 14 and only pH values at which DHBQ shows well-defined redox peaks are listed.

[b] DHBQ concentration is 1mM; sweep rate is 10mV/s and all potentials are iR-corrected.

Table S3. The diffusion coefficient (D) and electron-transfer rate constant (k^o) of presentative redox couples at glassy carbon electrode

Redox couple	D (cm^2/s)	k^o(cm/s)	Ref
FcNCl	$3.74*10^{-6}$	$3.66*10^{-5}$	[13]
FcN_2Br_2	$3.64*10^{-6}$	$4.60*10^{-6}$	[13]
alloxazine	-	$1.2*10^{-5}$	[11]
V^{3+}/V^{2+}	$4*10^{-6}$	$1.7*10^{-5}$	[14]
VO^{2+}/VO_2^{+}	$1.4*10^{-6}$	$7.5*10^{-4}$	[15]
DHBQ	$3.66*10^{-6}$	$2.12*10^{-3}$	this work

Table S4 Parameters for commercial Nafion membranes (data acquired from official distributors, except EIS resistance)

Membrane	N212	N115	N117
Ion exchange capacity (meq/g)	0.95~1.01 0.92 min.	0.95~1.01 0.90 min.	0.95~1.01 0.90 min
Thickness (μm)	50.8	127	183
EIS resistance (Ω cm^2) [a]	1.10	2.11	2.60
Conductivity (mS/cm) [b]	102	100 min.	100 min.
Water Uptake (%)	50	38	38
Basis weight (g/m^2)	100	250	360
Pretreatment	DI soaked	DI soaked	DI soaked

[a]. Measured in this work, see Fig.S5.

[b]. Membrane conditioned in 100 °C water for 1 hr. Measurement cell submersed in 25 °C DI water during experiment. Membrane impedance (real) taken at zero imaginary impedance.

Table S5. Properties for Library of DHBQ Derivatives: Group 1

R_2, R_5	R_3	R_6	Predicted $2e^-$ Redox Potential[a] (V)	Predicted Oxidized Form LogS at pH=14[b]
-(O-CH_2CH_2)$_2$-OH	-$CH_2CH_2CH_3$	-$CH_2CH_2CH_3$	-0.31	-3.05
-H	-CH-(para$C_6H_4NH_2$)$_2$	-CH-(para$C_6H_4NH_2$)$_2$	-0.28	-6.58
-(O-CH_2CH_2)$_2$-OH	-CH-(para$C_6H_4NH_2$)$_2$	-CH-(para$C_6H_4NH_2$)$_2$	-0.28	-4.68
-(O-CH_2CH_2)$_2$-OH	-CH_3	-CH_3	-0.26	-0.76
-OH	-$CH_2N(CH_3)_2$	-$CH_2N(CH_3)_2$	-0.25	1.91
-(O-CH_2CH_2)$_2$-OH	CH_2CH_3	CH_2CH_3	-0.23	-2.06
-H	-CH-(meta$C_6H_4NH_2$)$_2$	-CH-(meta$C_6H_4NH_2$)$_2$	-0.23	-6.58
-(O-CH_2CH_2)$_2$-OH	-CH-(paraC_6H_4OH)$_2$	-CH-(paraC_6H_4OH)$_2$	-0.22	0.00
-OH	-$(CH_2OCH_2)_3$-OH	-$(CH_2OCH_2)_3$-OH	-0.21	2.65
-H	-CH-(paraC_6H_4OH)$_2$	-CH-(paraC_6H_4OH)$_2$	-0.21	0.00
-OH	-CH-(para$C_6H_4NH_2$)$_2$	-CH-(para$C_6H_4NH_2$)$_2$	-0.21	0.00
-(O-CH_2CH_2)$_2$-OH	-CH-(meta$C_6H_4NH_2$)$_2$	-CH-(meta$C_6H_4NH_2$)$_2$	-0.18	-4.68
-OH	-CH_2NH_2	-CH_2NH_2	-0.18	2.28
-(O-CH_2CH_2)$_2$-OH	-CH-(metaC_6H_4OH)$_2$	-CH-(metaC_6H_4OH)$_2$	-0.17	0.00
-OH	-CH-(paraC_6H_4OH)$_2$	-CH-(paraC_6H_4OH)$_2$	-0.17	0.00
-H	-CH-(C_6H_5)$_2$	-CH-(C_6H_5)$_2$	-0.16	-7.43
-OH	-$CH_2CH_2CH_3$	-$CH_2CH_2CH_3$	-0.16	0.00
-OH	-CH-(meta$C_6H_4NH_2$)$_2$	-CH-(meta$C_6H_4NH_2$)$_2$	-0.15	0.00
-(O-CH_2CH_2)$_2$-OH	-$CH_2N(CH_3)_2$	-$CH_2N(CH_3)_2$	-0.15	-0.20
-OH	-$(CH_2CH_2O)_3$-H	-$(CH_2CH_2O)_3$-H	-0.15	2.56
-OH	-CH_2CH_3	-CH_2CH_3	-0.15	0.14
-H	-CH-(metaC_6H_4OH)$_2$	-CH-(metaC_6H_4OH)$_2$	-0.15	0.00
-(O-CH_2CH_2)$_2$-OH	-CH_2NH_2	-CH_2NH_2	-0.14	0.08
-H	-$CH_2CH_2CH_3$	-$CH_2CH_2CH_3$	-0.14	-4.35
-OH	-$CH_2CH_2NH_2$	-$CH_2CH_2NH_2$	-0.14	2.45
-OH	-CH-(C_6H_5)$_2$	-CH-(C_6H_5)$_2$	-0.14	0.00
-H	-CH_2CH_3	-CH_2CH_3	-0.13	-3.31
-(O-CH_2CH_2)$_2$-OH	-CH-(C_6H_5)$_2$	-CH-(C_6H_5)$_2$	-0.13	-5.65
-OH	-CH_3	-CH_3	-0.12	1.49
-(O-CH_2CH_2)$_2$-OH	-$CH_2CH_2NH_2$	-$CH_2CH_2NH_2$	-0.12	0.30
-H	-$CH_2N(CH_3)_2$	-$CH_2N(CH_3)_2$	-0.11	-1.55
-OH	-metaC_6H_4OH	-metaC_6H_4OH	-0.11	0.00
-H	-$CH_2CH_2NH_2$	-$CH_2CH_2NH_2$	-0.11	-1.00
-H	-CH_3	-CH_3	-0.09	-1.95
-OH	-H	CH_2CH_3	-0.08	0.45
-OH	-H	-$CH_2CH_2CH_3$	-0.08	0.00

[a] Calculated vs. DHBQ using B3LYP/6-311+G(d,p) CPCM

[b] Calculated using ChemAxon suite

Table S6. Properties for Library of DHBQ Derivatives: Group 2

R_2, R_5	R_3	R_6	Predicted $2e^-$ Redox Potential[a] (V)	Predicted Oxidized Form LogS at pH=14[b]
-OH	-CH-(meta$C_6H_4OH)_2$	-CH-(meta$C_6H_4OH)_2$	-0.08	0.00
-(O-$CH_2CH_2)_2$-OH	-CH-(meta$C_6H_4NH_2)_2$	-CH-(meta$C_6H_4NH_2)_2$	-0.06	-4.96
-OH	-H	-$(CH_2OCH_2)_3$-OH	-0.06	1.57
-OH	-H	-metaC_6H_4OH	-0.06	0.00
-OH	-H	-CH_3	-0.06	1.13
-O-CH_2CH_2OH	-$CH_2N(CH_3)_2$	-$CH_2N(CH_3)_2$	-0.06	-0.24
-OH	-C_6H_5	-C_6H_5	-0.06	0.00
-OH	-metaC_6H_4OH	-metaC_6H_4OH	-0.05	0.00
-(O-$CH_2CH_2)_2$-OH	-CH-(ortho$C_6H_4NH_2)_2$	-CH-(ortho$C_6H_4NH_2)_2$	-0.05	-4.68
-OH	-H	-$(CH_2CH_2O)_3$-H	-0.04	1.58
-OH	-H	-C_6H_5	-0.04	0.00
-H	-CH_2NH_2	-CH_2NH_2	-0.03	-1.17
-OH	-H	-metaC_6H_4OH	-0.03	0.00
-OH	-H	-H	0.00	0.77
-OH	-H	-OH	0.00	1.49
-OH	-H	-$(CH_2CH_2O)_2$-H	0.01	1.62
-O-CH_2CH_2OH	-CH-(para$C_6H_4NH_2)_2$	-CH-(para$C_6H_4NH_2)_2$	0.02	-4.96
-OH	-$(CH_2CH_2O)_2$-H	-$(CH_2CH_2O)_2$-H	0.02	2.53
-O-CH_2CH_2OH	-CH-(ortho$C_6H_4NH_2)_2$	-CH-(ortho$C_6H_4NH_2)_2$	0.02	-4.95
-OH	-CH-(ortho$C_6H_4NH_2)_2$	-CH-(ortho$C_6H_4NH_2)_2$	0.03	0.00
-H	-CH-(ortho$C_6H_4NH_2)_2$	-CH-(ortho$C_6H_4NH_2)_2$	0.06	-6.58
-O-CH_2CH_2OH	-CH_2NH_2	-CH_2NH_2	0.08	0.08
-OH	-H	-CH_2CH_2OH	0.08	1.66
-OH	-H	-CH_2OH	0.09	1.58
-O-CH_2CH_2OH	-$CH_2CH_2NH_2$	-$CH_2CH_2NH_2$	0.09	0.28
-O-CH_2CH_2OH	-CH-(para$C_6H_4OH)_2$	-CH-(para$C_6H_4OH)_2$	0.11	0.00
-O-CH_2CH_2OH	-$CH_2CH_2CH_3$	-$CH_2CH_2CH_3$	0.13	-3.07
-O-CH_2CH_2OH	-CH-(meta$C_6H_4OH)_2$	-CH-(meta$C_6H_4OH)_2$	0.13	0.00
-O-CH_2CH_2OH	-CH-($C_6H_5)_2$	-CH-($C_6H_5)_2$	0.14	-5.87
-O-CH_2CH_2OH	-CH_2CH_3	-CH_2CH_3	0.14	-2.06
-OH	-CH_2OH	-CH_2OH	0.16	2.39
-O-CH_2CH_2OH	-CH_3	-CH_3	0.16	-0.73
-OH	-CH_2CH_2OH	-CH_2CH_2OH	0.18	2.57
-OH	-CH-(ortho$C_6H_4OH)_2$	-CH-(ortho$C_6H_4OH)_2$	0.32	0.00
-O-CH_2CH_2OH	-CH-(ortho$C_6H_4OH)_2$	-CH-(ortho$C_6H_4OH)_2$	0.38	0.00
-H	-CH-(ortho$C_6H_4OH)_2$	-CH-(ortho$C_6H_4OH)_2$	0.49	0.00

[a] Calculated vs. DHBQ using B3LYP/6-311+G(d,p) CPCM

[b] Calculated using ChemAxon suite

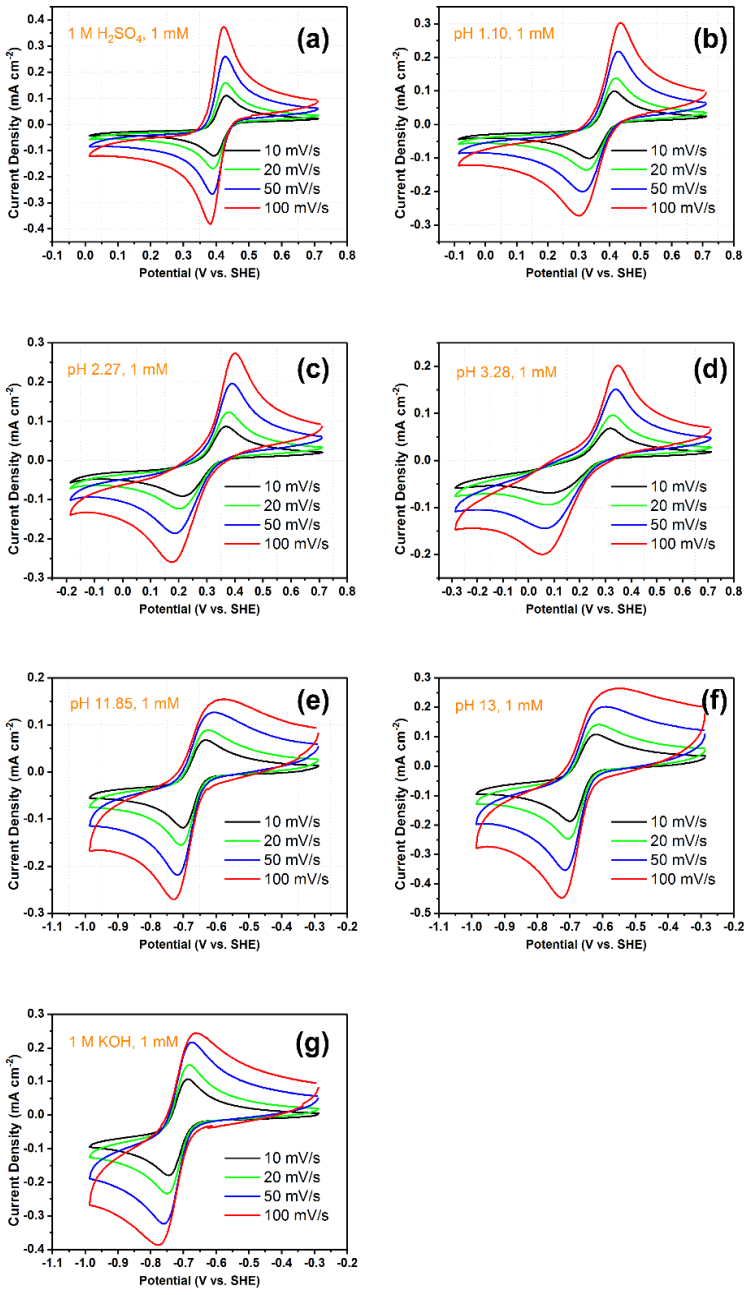

Figure S2. Cyclic voltammograms of 1 mM DHBQ solution at different pH with varied potential-scanning rates. For b-f, 1 M NaCl was used as the supporting electrolyte. The potential is reported relative to the standard hydrogen electrode (SHE) and is iR-corrected (pH 0.0, from 1 M H_2SO_4 and pH 14 from 1 M KOH).

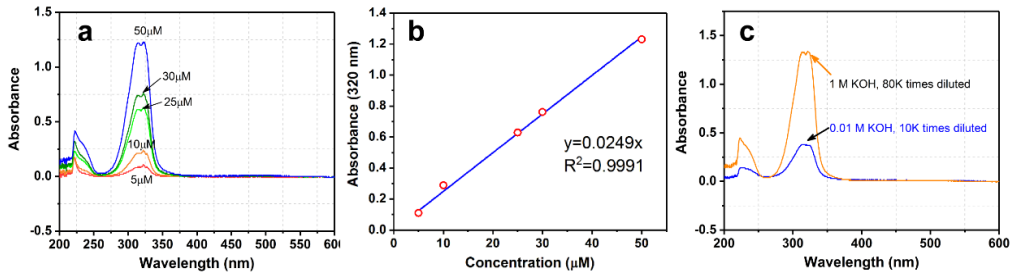

Figure S3. (a) UV-Vis spectra of DHBQ at different concentrations; (b) the absorbance at 320 nm versus the concentration; a least-squares linear fit to the data was performed to generate the calibration curve utilized in this work; (c) the absorbance of DHBQ solutions in 0.01 M KOH and 1 M KOH made by diluting saturated solutions by the ratio indicated in the figure, implying solubilities of 0.15 M and 4.31 M, respectively (note the redox electron concentrations are twice the molecule concentrations).

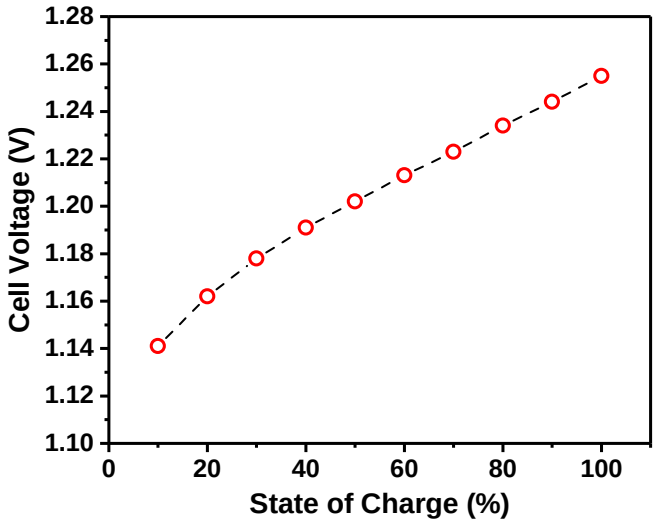

Figure S4. Open-circuit voltage of a DHBQ/$K_4Fe(CN)_6$ cell at pH 14 vs. state of charge

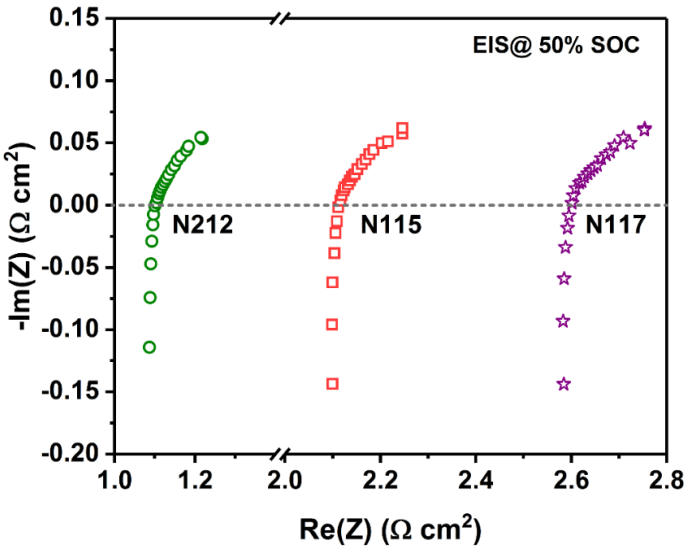

Figure S5. Electrochemical impedance spectroscopy (EIS) of Nafion 212, Nafion 115, and Nafion 117 inside a DHBQ/$K_4Fe(CN)_6$ cell at 50% SOC at frequencies ranging from 1 Hz – 10 kHz. The AC-ASR (high frequency resistance) of Nafion 212, Nafion 115 and Nafion 117 are 1.10, 2.11 and 2.60 $\Omega\,cm^2$, respectively.

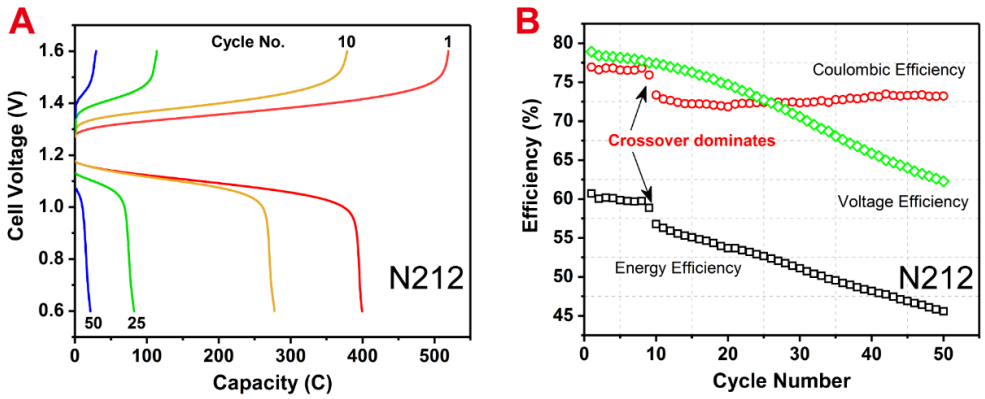

Figure S6. Cell cycling performance of a DHBQ/$K_4Fe(CN)_6$ cell with a Nafion 212 separator. The electrolytes comprise 6 mL of 0.5 M DHBQ in 2 M KOH and 22.5 mL of 0.4 M $K_4Fe(CN)_6$ in 1M KOH and the cells are cycled at 100 mA/cm^2 with potential cut-offs of 1.6V and 0.6 V. The potential was not maintained at the cut-off potentials once they were reached. For clarity, representative cell potential versus capacity curves (A) and efficiencies (coulombic efficiency, energy efficiency and voltage efficiency, B) over the whole cycling process are presented.

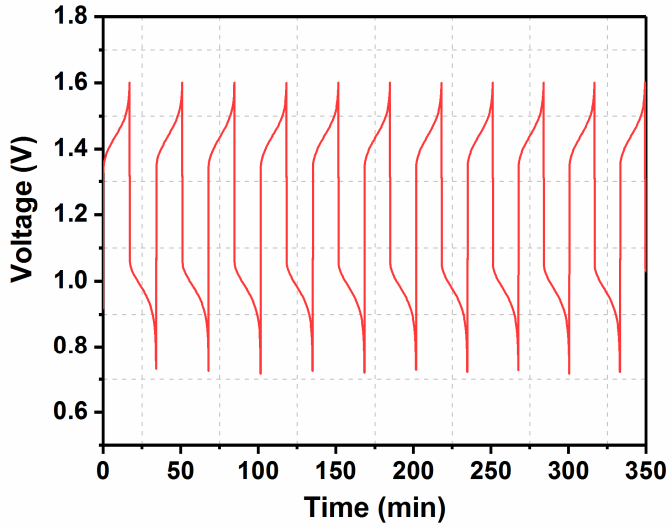

Figure S7. Representative voltage vs. time curves during cycling at 100 mA cm^{-2} for DHBQ/$K_4Fe(CN)_6$ cell with N115 membrane.

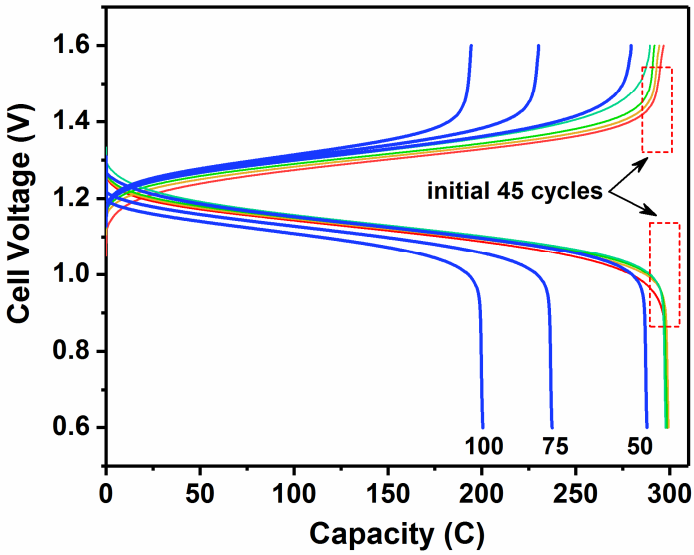

Figure S8. Cell potential versus capacity of a DHBQ/$K_4Fe(CN)_6$ cell with a Nafion 115 separator. The electrolytes comprise 6 mL of 0.5 M DHBQ in 2 M KOH and 7.5 mL of 0.4 M $K_4Fe(CN)_6$ in 1M KOH and the cells are cycled at 100 mA/cm^2 with potential cut-offs of 1.6 V and 0.6 V. The potential was not maintained at the cut-off potentials once they were reached. Representative cell potential versus capacity curves are presented (cycle #1, #10, #20, #45, #50, #75 and #100 are presented).

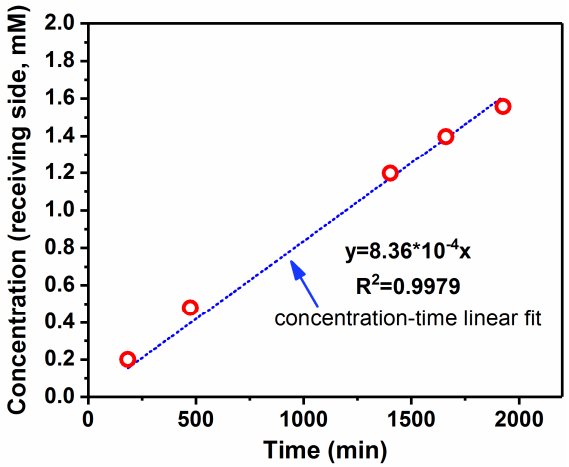

Figure S9. Crossover test of DHBQ across a Nafion 115 membrane. The line shows a least-squares linear fit to the data. The permeability is calculated from the rate of increase in concentration of DHBQ in the receiving reservoir.

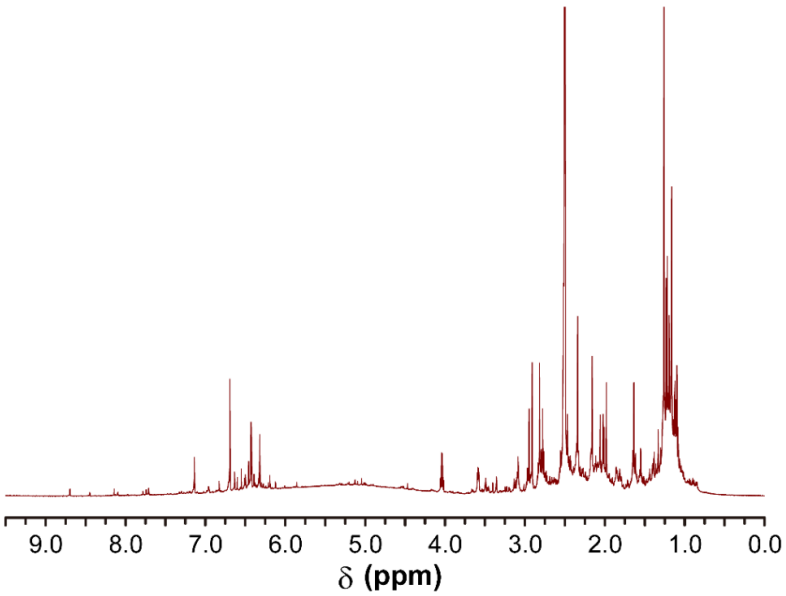

Figure S10. A typical ^{1}H-NMR spectrum recorded in DMSO-d_6 for DHBQ after cell cycling. After prolonged cell cycling, the anolyte reservoir was neutralized with HCl and evaporated under vacuum at 40 °C. The remaining solids were dissolved in DMSO-d_6.

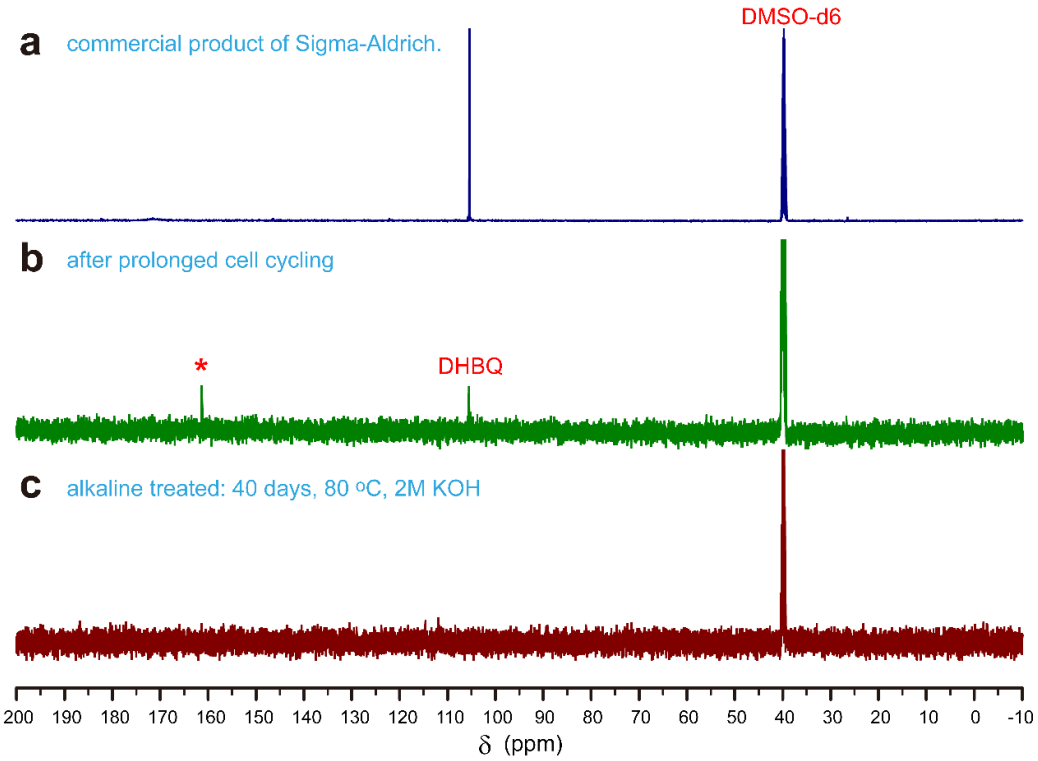

Figure S11. ^{13}C NMR of (a) commercial DHBQ from Sigma-Aldrich, (b) the DHBQ anolyte after prolonged cell cycling and (c) 2 M KOH–treated DHBQ at 80 °C after 40 days. The asterisk indicates the appearance of a new carbon signal. All spectra were recorded in DMSO-d_6 on Varian INOVA 500 spectrometers (500 MHz for ^{1}H, 125 MHz for ^{13}C). During ex-situ alkaline treatments, the sample solutions (10 mL, flushed with N_2 for 15 mins) were kept in a glass vial (20 mL), sealed with PTFE tape and parafilm.

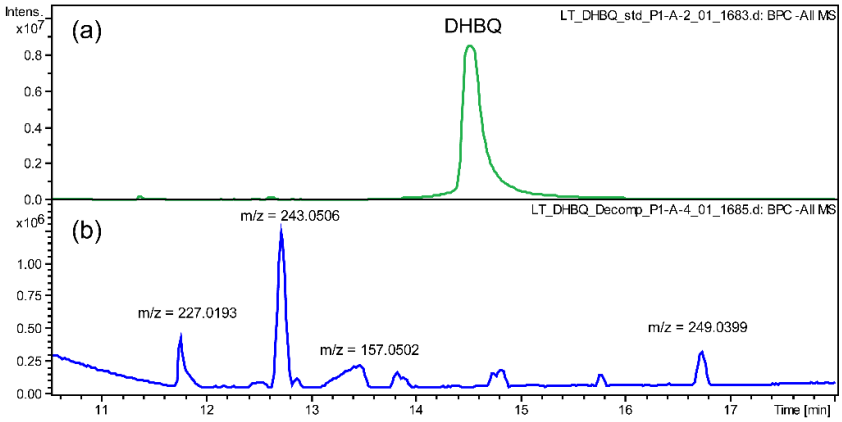

Figure S12. (a) Base Peak Chromatograph of DHBQ standard and (b) DHBQ treated in pH14 KOH solution for 40 days. Mass with highest intensity in representative decomposition peak was annotated above the corresponding peak (within 5 ppm error and correct isotopic pattern).

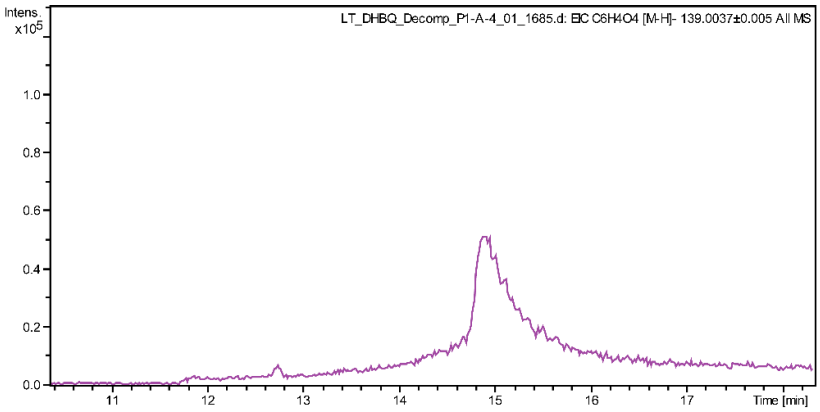

Figure S13. Extracted ion chromatograph ($C_6H_4O_4$ [M-H]$^-$) of decomposed DHBQ.

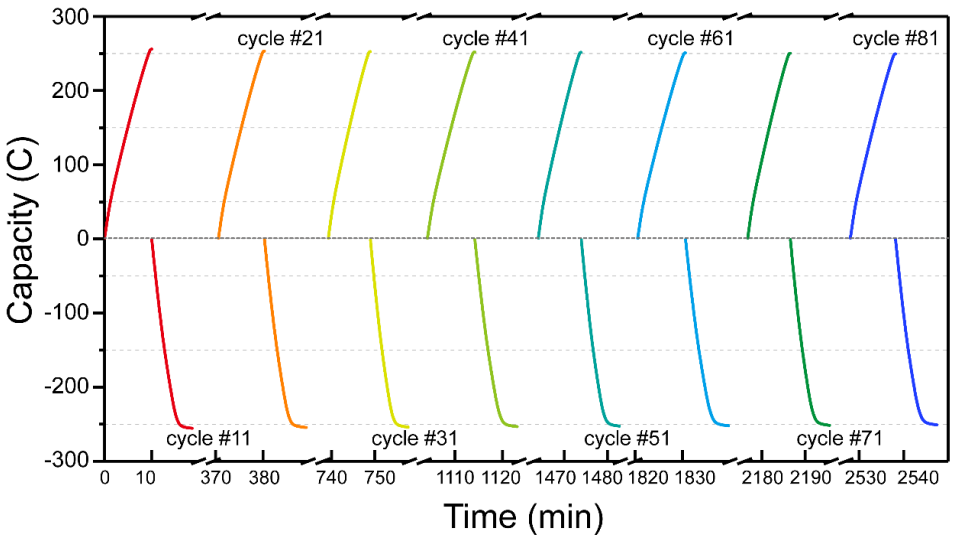

Figure S14. Capacity (positive values for charging, negative values for discharging) as a function of time for a DHBQ/$K_4Fe(CN)_6$ cell run at pH 12 (The volume of the posolyte is 22.5 mL(0.4M) and the negolyte is 6 mL(saturated). The membrane is N115.). The cell was cycled at 40 mA/cm^2. Every 10 cycles, a full charge-discharge cycle was conducted with voltage cut-offs of 1.6 V and 0.6 V, which was maintained at the end of each charge or discharge cycle until the current fell below 2 mA/cm^2. The plotted data are from each (10*n* + 1)st cycle and represent a full charge-discharge cycle after every 10 consecutive galvanostatic cycles.

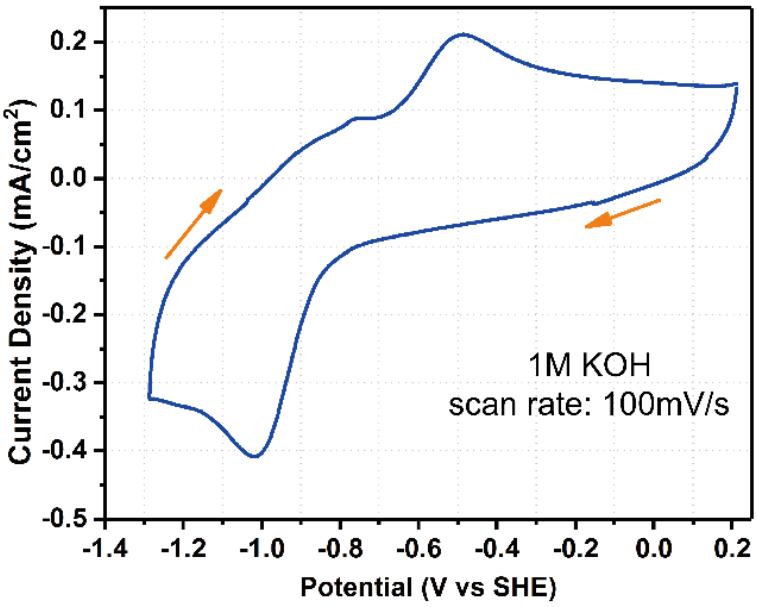

Figure S15. Cyclic voltammogram of 3,6-bis(diphenylmethyl)-2,5-dihydroxy-1,4-benzoquinone (DPM-DHBQ) recorded in 1 M KOH. The potential is referenced to the standard hydrogen electrode (SHE) and the potential sweep rate is 100 mV/s. The CV is reproducible in repeated scans and only one curve is presented for clarity (the 10th scan).

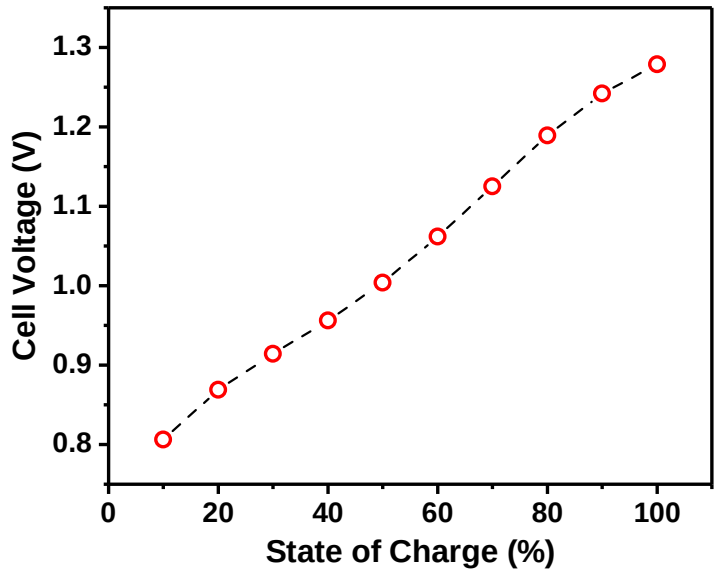

Figure S16. Open-circuit voltage of a polyBQ /$K_3Fe(CN)_6$cell at pH 14 at different states of charge

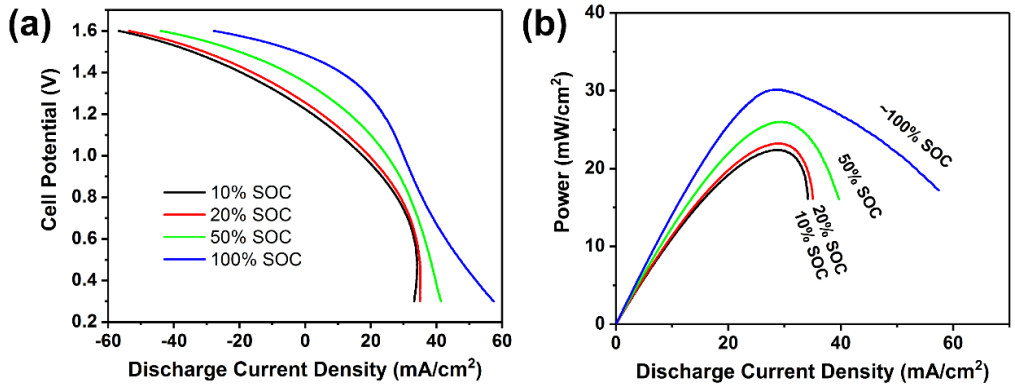

Figure S17. Electrochemical performance of a polyBQ/$K_3Fe(CN)_6$ cell using a Nafion 115 membrane. The polarization curves include (a) potential and (b) peak-power density versus discharge current density at 10%, 20%, 50% and ~100% state of charge, respectively.

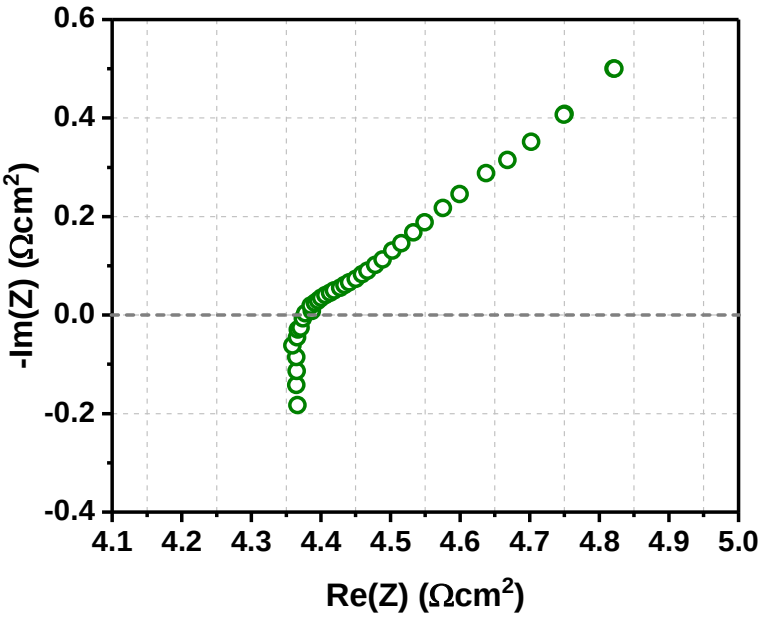

Figure S18. Electrochemical impedance spectroscopy (EIS) of Nafion 115 inside a polyBQ/$K_3Fe(CN)_6$ cell at frequencies ranging from 1 Hz to10 kHz. The AC-ASR (high frequency resistance) is 4.35 Ωcm^2.

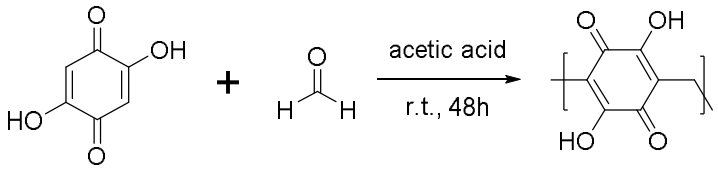

Figure S19. Synthesis of poly(2,5-dihydroxy-1,4-benzoquinone-3,6-methylene) via acid-catalyzed condensation of DHBQ with formaldehyde [16].

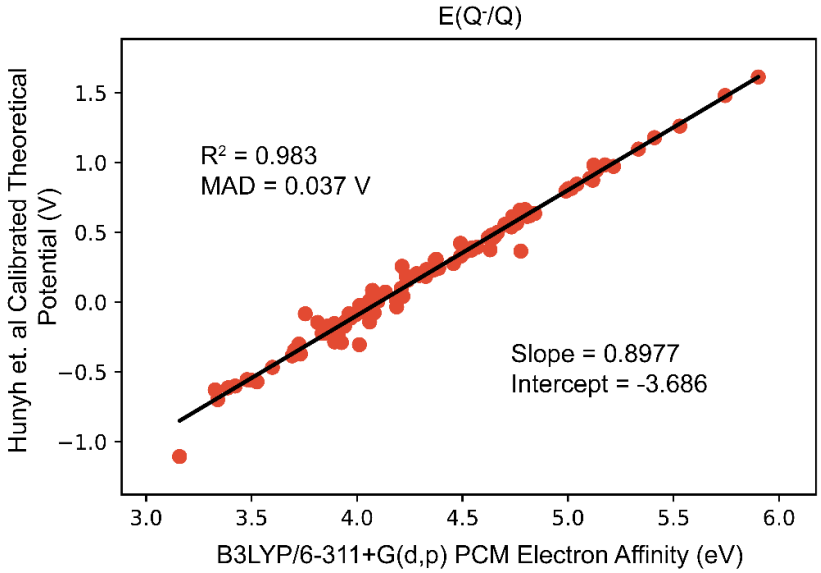

Figure S20. Calibration of single point B3LYP/6-311+G(d,p) PCM electron affinities (horizontal axis) vs. B3LYP/6-31++G(d,p) PCM optimized + zero-point calibrated redox potentials (vertical axis) for the first reduction of the quinones studied by Hunyh et al.[6], excluding thiol and carboxylic acid functionalization.

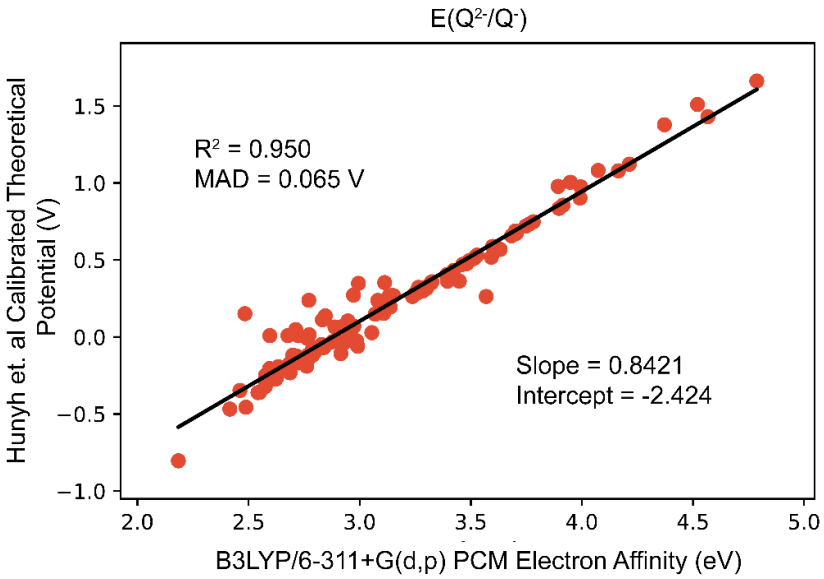

Figure S21. Calibration of single point B3LYP/6-311+G(d,p) PCM electron affinities (horizontal axis) vs. B3LYP/6-31++G(d,p) PCM optimized + zero-point calibrated redox potentials (vertical axis) for the second reduction of the quinones studied by Hunyh et al.[6], excluding thiol and carboxylic acid functionalization.

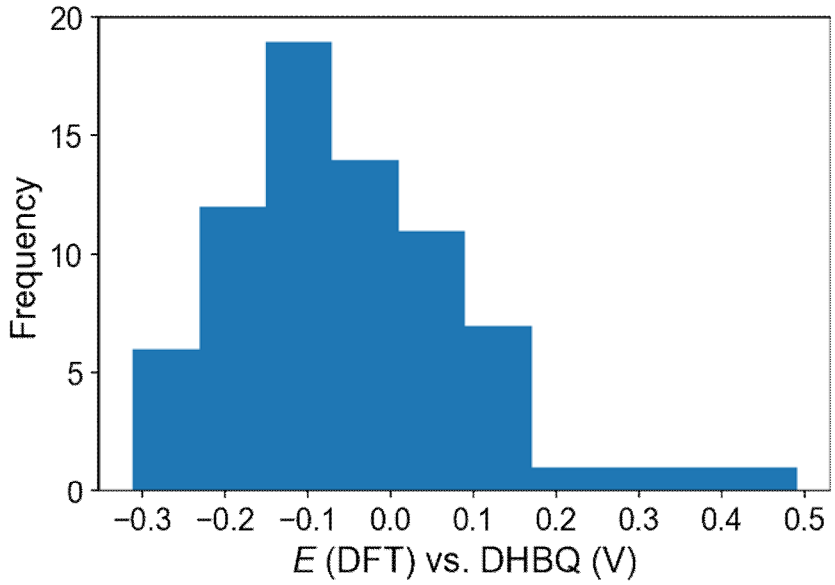

Figure S22. Distribution of DFT calculated reduction potentials of screening library vs. DHBQ.

References

[1] A. W. Misiolek, A. S. Ichimura, R. A. Gentner, R. H. Huang, V. P. McCaffrey, J. E. Jackson, *Inorg. Chem.* **2009**, 48, 9005.

[2] S. I. Sadykh-Zade, A. V. Ragimov, S. S. Suleimanova, V. I. Liogon'kii, *Polymer Science U.S.S.R.* **1972**, 14, 1395.

[3] a) T. Janoschka, N. Martin, U. Martin, C. Friebe, S. Morgenstern, H. Hiller, M. D. Hager, U. S. Schubert, *Nature* **2015**, 527, 78; b) A. Orita, M. G. Verde, M. Sakai, Y. S. Meng, *Nat Commun* **2016**, 7, 13230.

[4] E. S. Beh, D. De Porcellinis, R. L. Gracia, K. T. Xia, R. G. Gordon, M. J. Aziz, *ACS Energy Letters* **2017**, 2, 639.

[5] Y. Shao, Z. Gan, E. Epifanovsky, A. T. Gilbert, M. Wormit, J. Kussmann, A. W. Lange, A. Behn, J. Deng, X. Feng, *Mol. Phys.* **2015**, 113, 184.

[6] M. T. Huynh, C. W. Anson, A. C. Cavell, S. S. Stahl, S. Hammes-Schiffer, *J. Am. Chem. Soc.* **2016**, 138, 15903.

[7] M. Calculator Plugins were used for structure property prediction and calculation, 2016, ChemAxon (http://www.chemaxon.com).

[8] K. Lin, Q. Chen, M. R. Gerhardt, L. Tong, S. B. Kim, L. Eisenach, A. W. Valle, D. Hardee, R. G. Gordon, M. J. Aziz, M. P. Marshak, *Science* **2015**, 349, 1529.

[9] B. Huskinson, M. P. Marshak, C. Suh, S. Er, M. R. Gerhardt, C. J. Galvin, X. Chen, A. Aspuru-Guzik, R. G. Gordon, M. J. Aziz, *Nature* **2014**, 505, 195.

[10] a) T. Janoschka, N. Martin, M. D. Hager, U. S. Schubert, *Angew. Chem. Int. Ed. Engl.* **2016**, 55, 14427; b) T. Liu, X. Wei, Z. Nie, V. Sprenkle, W. Wang, *Adv. Energy Mater.* **2016**, 6, 1501449.

[11] K. Lin, R. Gómez-Bombarelli, E. S. Beh, L. Tong, Q. Chen, A. Valle, A. Aspuru-Guzik, M. J. Aziz, R. G. Gordon, *Nature Energy* **2016**, 1, 16102.

[12] J. Winsberg, C. Stolze, S. Muench, F. Liedl, M. D. Hager, U. S. Schubert, *ACS Energy Letters* **2016**, 1, 976.

[13] B. Hu, C. DeBruler, Z. Rhodes, T. L. Liu, *J. Am. Chem. Soc.* **2017**, 139, 1207.

[14] E. Sum, M. Skyllas-Kazacos, *J. Power Sources* **1985**, 15, 179.

[15] E. Sum, M. Rychcik, M. Skyllas-kazacos, *J. Power Sources* **1985**, 16, 85.

[16] T. Le Gall, K. H. Reiman, M. C. Grossel, J. R. Owen, *J. Power Sources* **2003**, 119-121, 316.